# The effect of μ-CN linkage isomerism and ancillary ligand set on directional metal–metal charge-transfer in cyanide-bridged dimanganese complexes†‡

**Christopher J. Adams, Kirsty M. Anderson, Neil G. Connelly,* Estefania Llamas-Rey, A. Guy Orpen and Rowena L. Paul**

***Received 20th April 2007, Accepted 19th June 2007***
***First published as an Advance Article on the web 5th July 2007***
**DOI: 10.1039/b705975b**



The reaction of [Mn(CN)L′(NO)(η⁵-$C_5R_4$Me)] with *cis*- or *trans*-[MnBrL(CO)$_2$(dppm)], in the presence of Tl[$PF_6$], gives homobinuclear cyanomanganese(I) complexes *cis*- or *trans*-[(dppm)(CO)$_2$LMn(μ-NC)MnL′(NO)(η⁵-$C_5R_4$Me)]⁺, linkage isomers of which, *cis*- or *trans*-[(dppm)(CO)$_2$LMn(μ-CN)MnL′(NO)(η⁵-$C_5R_4$Me)]⁺, are synthesised by reacting *cis*- or *trans*-[Mn(CN)L(CO)$_2$(dppm)] with [MnIL′(NO)(η⁵-$C_5R_4$Me)] in the presence of Tl[$PF_6$]. X-Ray structural studies on the isomers *trans*-[(dppm)(CO)$_2${(EtO)$_3$P}Mn(μ-NC)Mn(CNBu$^t$)(NO)-(η⁵-$C_5H_4$Me)]⁺ and *trans*-[(dppm)(CO)$_2${(EtO)$_3$P}Mn(μ-CN)Mn(CNBu$^t$)(NO)(η⁵-$C_5H_4$Me)]⁺ show nearly identical molecular structures whereas *cis*-[(dppm)(CO)$_2${(PhO)$_3$P}Mn(μ-NC)Mn-{P(OPh)$_3$}(NO)(η⁵-$C_5H_4$Me)]⁺ and *cis*-[(dppm)(CO)$_2${(PhO)$_3$P}Mn(μ-CN)Mn-{P(OPh)$_3$}(NO)(η⁵-$C_5H_4$Me)]⁺ differ, effectively in the *N*- and *C*-coordination respectively of two different optical isomers of the *pseudo*-tetrahedral units (NC)Mn{P(OPh)$_3$}(NO)(η⁵-$C_5H_4$Me) and (CN)Mn{P(OPh)$_3$}(NO)(η⁵-$C_5H_4$Me) to the octahedral manganese centre. Electrochemical and spectroscopic studies on [(dppm)(CO)$_2$LMn(μ-XY)MnL′(NO)(η⁵-$C_5R_4$Me)]⁺ show that systematic variation of the ligands L and L′, of the cyclopentadienyl ring substituents R, and of the μ-CN orientation (XY = CN or NC) allows control of the order of oxidation of the two metal centres and hence the direction and energy of metal–metal charge-transfer (MMCT) through the cyanide bridge in the mixed-valence dications. Chemical one-electron oxidation of *cis*- or *trans*-[(dppm)(CO)$_2$LMn(μ-NC)MnL′(NO)(η⁵-$C_5R_4$Me)]⁺ with [NO][$PF_6$] gives the mixed-valence dications *trans*-[(dppm)(CO)$_2$LMn$^{II}$(μ-NC)Mn$^{I}$L′(NO)(η⁵-$C_5R_4$Me)]²⁺ which show solvatochromic absorptions in the electronic spectrum, assigned to optically induced Mn(I)-to-Mn(II) electron transfer *via* the cyanide bridge.

## Introduction

In our studies of the construction and properties of cyanide-bridged complexes containing redox-active units such as **A**–**C** (Scheme 1) we have previously investigated two series of complexes in which linking two of the same or very similar mononuclear units (*i.e.* two of the octahedral units, **A** and/or **B**, or two of the tetrahedral units, **C**) gives linkage isomers (due to the asymmetry of the cyanide bridge), *i.e.* [(L-L)LMn(μ-CN)MnL′(NO)(L′-L′)][$PF_6$] {L or L′ = P(OPh)$_3$, P(OEt)$_3$ or $PEt_3$; L-L or L′-L′ = dppm or dppe}[1,2] and [(η⁵-$C_5H_4$Me)(NO)LMn(μ-CN)MnL′(NO)(η⁵-$C_5H_4$Me)][$PF_6$] (L or L′ = $PPh_3$, CNBu$^t$ or CNXyl).[3] Varying the ancillary ligands at each metal centre then allows fine tuning of the energy of intramolecular metal–metal charge-transfer (MMCT) and thence electronic properties such as solvatochromism.

We now give details[4] of a third series of complexes, [(dppm)(CO)$_2$LMn(μ-XY)MnL′(NO)(η⁵-$C_5R_4$Me)]⁺ (XY = CN or NC) in which one octahedral unit (based on **A** or **B**) and one *pseudo*-tetrahedral unit (based on **C**) are linked. The order of one-electron oxidation of the two metal centres in the monocations, and hence the direction and energy of metal–metal charge-transfer (MMCT) in the corresponding mixed-valence dications, can be controlled by the systematic variation of the ligands at either manganese atom, the *cis* or *trans* arrangement of the Mn(CO)$_2$ fragment, the substitution pattern in the η⁵-$C_5R_4$Me ring, and the orientation of the cyanide bridge.

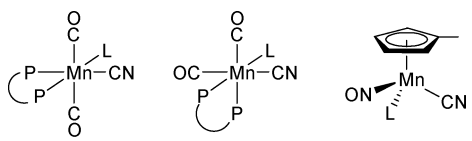


**Scheme 1** P–P = $Ph_2PCH_2PPh_2$ = dppm.

## Results and discussion

### The synthesis and spectroscopic characterisation of linkage isomers

The room temperature reaction of the *pseudo*-tetrahedral cyanomanganese complexes [Mn(CN)L′(NO)(η⁵-$C_5R_4$Me)]

*School of Chemistry, University of Bristol, Bristol, UK, BS8 1TS. E-mail: neil.connelly@bristol.ac.uk; Fax: +44 (0)117 929 0509; Tel: +44 (0)117 928 8162*

† CCDC reference numbers 166635, 166636, 644601–644604. For crystallographic data in CIF or other electronic format see DOI: 10.1039/b705975b

‡ Electronic supplementary information (ESI) available: Metal-to-metal charge-transfer data. See DOI: 10.1039/b705975b

{R = H, L′ = $PPh_3$, $P(OPh)_3$, $CNBu^t$ or CNXyl; R = Me, L = $CNBu^t$} with octahedral *cis*- or *trans*-$[MnBrL(CO)_2(dppm)]$ {L = $P(OPh)_3$ or $P(OEt)_3$} in the presence of $Tl[PF_6]$ in $CH_2Cl_2$ gave orange or red solutions from which *cis*- or *trans*-$[(dppm)(CO)_2LMn(\mu\text{-}NC)MnL'(NO)(\eta^5\text{-}C_5R_4Me)][PF_6]$ $\mathbf{1}^+[PF_6]^-$–$\mathbf{10}^+[PF_6]^-$ (Scheme 2) were isolated as yellow to red microcrystalline solids. In some cases, the attempted synthesis of *trans*-$Mn(CO)_2$ complexes gave inseparable mixtures of *cis*- and *trans*-$Mn(CO)_2$ isomers, necessitating an alternative preparative route. Thus, for example, *trans*-$\mathbf{7}^+$ was synthesised by one-electron oxidation of *cis*-$\mathbf{7}^+$ with $[NO][PF_6]$ and *in situ* reduction with $N_2H_4{\cdot}xH_2O$ of the dication, *trans*-$\mathbf{7}^{2+}$, formed by redox-induced *cis*–*trans* isomerisation.[5]

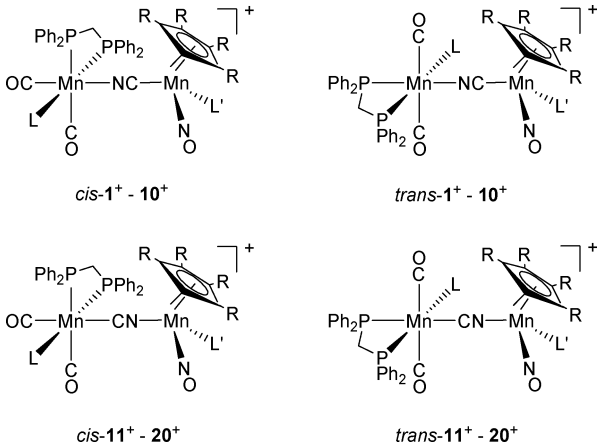


**Scheme 2** Complexes *cis*- and *trans*-$\mathbf{1}^+$–$\mathbf{20}^+$ (*cis* or *trans* refers to the relative arrangement of the two carbonyl ligands at the octahedral manganese centre).

The linkage isomers of $\mathbf{1}^+$–$\mathbf{10}^+$, *i.e.* *cis*- and *trans*-$[(dppm)(CO)_2LMn(\mu\text{-}CN)MnL'(NO)(\eta^5\text{-}C_5R_4Me)][PF_6]$ $\mathbf{11}^+[PF_6]^-$–$\mathbf{20}^+[PF_6]^-$ (Scheme 2), were synthesised by the room temperature reaction of the octahedral cyanomanganese ligands *cis*- or *trans*-$[Mn(CN)L(CO)_2(dppm)]$ {L = $P(OPh)_3$ or $P(OEt)_3$} with the *pseudo*-tetrahedral iodide complexes $[MnIL'(NO)(\eta^5\text{-}C_5R_4Me)]$ {R = H, L′ = $PPh_3$, $P(OPh)_3$, $CNBu^t$ or CNXyl; R = Me, L′ = $CNBu^t$} in the presence of $Tl[PF_6]$ in $CH_2Cl_2$. Alternatively, *cis*-$\mathbf{15}^+$ and *cis*- and *trans*-$[(dppm)(CO)_2\{(RO)_3P\}Mn(\mu\text{-}CN)Mn(CNBu^t)(NO)(\eta^5\text{-}C_5H_4Me)]^+$ (R = Ph $\mathbf{19}^+$ or Et $\mathbf{20}^+$) were synthesised by the reaction of *cis*-$[Mn(CN)\{P(OR)_3\}(CO)_2(dppm)]$ with $[Mn(CO)L(NO)(\eta^5\text{-}C_5H_4Me)][PF_6]$ (L = $PPh_3$ or $CNBu^t$) in the presence of $Me_3NO$. Analytical data for *cis*- and *trans*-$\mathbf{1}^+[PF_6]^-$–$\mathbf{20}^+[PF_6]^-$ are given in Table 1.

In $CH_2Cl_2$ the IR spectra (Table 1) of $\mathbf{1}^+$–$\mathbf{20}^+$ show increases in $\nu$(CN) of 20–30 $cm^{-1}$ compared with the mononuclear cyanomanganese precursors $[Mn(CN)L'(NO)(\eta^5\text{-}C_5R_4Me)]$ and $[Mn(CN)L(CO)_2(dppm)]$. Though such shifts to higher energy have been usually attributed to the kinematic effect of constraining the CN motion by *N*-coordination to a second metal fragment,[6] a recent theoretical study[7] has shown this factor to be rather less important than others such as σ-bonding and cation charge.

The number of carbonyl stretching bands observed for $[(dppm)(CO)_2LMn(\mu\text{-}XY)MnL'(NO)(\eta^5\text{-}C_5R_4Me)]^+$ $\mathbf{1}^+$–$\mathbf{20}^+$ depends on the geometry of the $Mn(CO)_2$ unit; two are observed for *cis*-$Mn(CO)_2$ and one for *trans*-$Mn(CO)_2$ species (with a very weak second band observed at higher energy for the symmetry forbidden A-mode). This, and the observation of redox-induced *cis*–*trans* isomerisation on oxidation,[5] provides a useful diagnostic tool for identifying the order of oxidation of the two redox-active centres in $\mathbf{1}^+$–$\mathbf{20}^+$.

The IR spectra show not only that linkage isomers such as $\mathbf{1}^+$ and $\mathbf{11}^+$ are distinguishable but also that they are stable to isomerisation (*cf.* the more ready isomerisation of species such as $[(Ph_3P)Au(\mu\text{-}CN)RhCl_2(PMe_2Ph)_3]^+$ and $[(OC)_5W(\mu\text{-}NC)Cu(PPh_3)_3]$ to $[(Ph_3P)Au(\mu\text{-}NC)RhCl_2(PMe_2Ph)_3]^+$[8] and $[(OC)_5W(\mu\text{-}CN)Cu(PPh_3)_3]$[9] respectively). In general, the $\nu$(NO) band appears at approximately 10 $cm^{-1}$ higher energy when the *pseudo*-tetrahedral Mn centre is bound to the better π-accepting *C*-end of the bridging cyanide {compare $\nu$(NO) = 1742 $cm^{-1}$ for *cis*-$\mathbf{1}^+$ with $\nu$(NO) = 1734 $cm^{-1}$ for the linkage isomer *cis*-$\mathbf{11}^+$}. Conversely, the $\nu$(CO) bands appear at lower energy when the octahedral centre is bound to the better σ-donating *N*-end of the bridge. {Compare $\nu$(CO) = 1971, 1905 $cm^{-1}$ for *cis*-$\mathbf{1}^+$ with $\nu$(CO) = 1974, 1920 $cm^{-1}$ for *cis*-$\mathbf{11}^+$.}

## The X-ray structures of *cis*-$\mathbf{2}^+$, *trans*-$\mathbf{7}^+$, *cis*-$\mathbf{8}^+$, *cis*-$\mathbf{9}^+$, *cis*-$\mathbf{12}^+$ and *trans*-$\mathbf{17}^+$

As far as we are aware, only two pairs of stable dinuclear complexes showing cyanide–isocyanide linkage isomerism have been previously structurally characterised, namely $[(H_3N)_5Co(\mu\text{-}XY)Co(CN)_5]$ (XY = CN and NC)[10] and $[(OC)_5Cr(\mu\text{-}XY)Fe(dppe)(\eta^5\text{-}C_5H_5)]$ (XY = CN and NC).[11] Structural analyses of two pairs of the new linkage isomers, namely *trans*-$[(dppm)(CO)_2\{(EtO)_3P\}Mn(\mu\text{-}XY)Mn(CNBu^t)(NO)(\eta^5\text{-}C_5H_4Me)]^+$ (XY = NC, *trans*-$\mathbf{7}^+$; XY = CN, *trans*-$\mathbf{17}^+$), and *cis*-$[(dppm)(CO)_2\{(PhO)_3P\}Mn(\mu\text{-}XY)Mn\{P(OPh)_3\}(NO)(\eta^5\text{-}C_5H_4Me)]^+$ (XY = NC, *cis*-$\mathbf{2}^+$; XY = CN, *cis*-$\mathbf{12}^+$) were therefore carried out in order to investigate possible changes arising from μ-CN isomerism.

The structures of the cations *trans*-$\mathbf{17}^+$ (also representative of *trans*-$\mathbf{7}^+$, see below), *cis*-$\mathbf{2}^+$ and *cis*-$\mathbf{12}^+$ are shown in Fig. 1–3 respectively; selected bond lengths and angles are given in Table 2 (for *trans*-$\mathbf{7}^+$ and *trans*-$\mathbf{17}^+$) and Table 3 (for *cis*-$\mathbf{2}^+$ and for the two crystallographically independent units of *cis*-$\mathbf{12}^+$). Dinuclear complexes containing the cyanomanganese ligands $[Mn(CN)(CNXyl)(NO)(\eta^5\text{-}C_5H_4Me)]$ and $[Mn(CN)(CNBu^t)(NO)(\eta^5\text{-}C_5Me_5)]$, namely *cis*-$[(dppm)(CO)_2\{(EtO)_3P\}Mn(\mu\text{-}NC)Mn(CNXyl)(NO)(\eta^5\text{-}C_5H_4Me)]^+$ *cis*-$\mathbf{8}^+$ (Fig. 4) and *cis*-$[(dppm)(CO)_2\{(PhO)_3P\}Mn(\mu\text{-}NC)Mn(CNBu^t)(NO)(\eta^5\text{-}C_5Me_5)]^+$ *cis*-$\mathbf{9}^+$ (Fig. 5), have also been structurally characterised. Selected bond lengths and angles are given in Table 4.

Each of the cations *trans*-$\mathbf{7}^+$, *trans*-$\mathbf{17}^+$, *cis*-$\mathbf{2}^+$, *cis*-$\mathbf{12}^+$, *cis*-$\mathbf{8}^+$ and *cis*-$\mathbf{9}^+$ contains two manganese centres linked by a nearly linear Mn–CN–Mn bridge, with Mn–C–N and C–N–Mn angles ranging from 171.6 to 179.1°. The geometries of the $[MnXL(CO)_2(dppm)]$ and $[MnYL'(NO)(\eta^5\text{-}C_5R_4Me)]$ fragments are octahedral and *pseudo*-tetrahedral respectively (from now on designated as $Mn_{oct}$ and $Mn_{tet}$).

For a given pair of linkage isomers, the Mn–CN bond length appears shorter than Mn–NC {*cf.* $Mn_{tet}$–CN = 1.951(3) Å in *trans*-$\mathbf{7}^+$ *vs.* $Mn_{tet}$–NC = 1.968(3) Å in *trans*-$\mathbf{17}^+$, and CN–$Mn_{oct}$ = 2.010(3) Å in *trans*-$\mathbf{7}^+$ *vs.* NC–$Mn_{oct}$ = 1.955(3) Å in *trans*-$\mathbf{17}^+$}, indicating the better π-accepting ability of a *C*-donor fragment.

 

**Table 1** Analytical and IR spectroscopic data for *cis*- and *trans*-[(dppm)(CO)$_2$LMn(μ-XY)MnL′(NO)(η$^5$-C$_5$R$_4$Me)][PF$_6$]

| | | | | | | | Analysis (%)[b] | | | IR[c]/cm$^{-1}$ | | | |
|---|---|---|---|---|---|---|---|---|---|---|---|---|---|
| Complex[a] | XY | L | L′ | R | Colour | Yield (%) | C | H | N | ν(CNR) | ν(CN) | ν(CO) | ν(NO) |
| *cis*-**1**$^+$ | NC | P(OPh)$_3$ | PPh$_3$ | H | Orange | 63 | 59.7 (59.9) | 4.4 (4.2) | 2.0 (2.0) | — | 2109w | 1971, 1905 | 1742 |
| *trans*-**1**$^+$ | NC | P(OPh)$_3$ | PPh$_3$ | H | Orange | 68 | 59.6 (59.9) | 4.1 (4.2) | 2.2 (2.0) | — | 2116w | 2018w, 1930 | 1741 |
| *cis*-**2**$^+$ | NC | P(OPh)$_3$ | P(OPh)$_3$ | H | Orange | 62 | 58.0 (58.0) | 3.6 (4.1) | 2.2 (1.9) | — | 2127w | 1971, 1905 | 1763 |
| *trans*-**2**$^+$ | NC | P(OPh)$_3$ | P(OPh)$_3$ | H | Orange | 59 | 58.0 (58.0) | 4.2 (4.1) | 2.2 (1.9) | — | 2127w | 2018w, 1930 | 1763 |
| *cis*-**3**$^+$ | NC | P(OPh)$_3$ | CNBu$^t$ | H | Orange | 71 | 56.4 (55.9) | 4.7 (4.4) | 3.6 (3.4) | 2168m | 2130w | 1971, 1908 | 1764 |
| *trans*-**3**$^+$ | NC | P(OPh)$_3$ | CNBu$^t$ | H | Orange | 45 | 55.6 (55.9) | 4.4 (4.4) | 3.6 (3.4) | 2167m | 2132w | 2020w, 1932 | 1762 |
| *cis*-**4**$^+$ | NC | P(OPh)$_3$ | CNXyl | H | Orange | 75 | 57.9 (57.6) | 4.3 (4.2) | 3.3 (3.3) | 2147m | 2130w | 1970, 1908 | 1766 |
| *trans*-**4**$^+$ | NC | P(OPh)$_3$ | CNXyl | H | Orange | 54 | 57.9 (57.6) | 4.3 (4.2) | 3.2 (3.3) | 2146m | 2132w | 2019w, 1932 | 1765 |
| *cis*-**5**$^+$ | NC | P(OEt)$_3$ | PPh$_3$ | H | Orange | 66 | 55.1 (55.3) | 4.7 (4.7) | 2.5 (2.2) | — | 2102w | 1959, 1894 | 1743 |
| *trans*-**5**$^+$ | NC | P(OEt)$_3$ | PPh$_3$ | H | Orange | 59 | 55.5 (55.3) | 4.6 (4.7) | 2.3 (2.2) | — | 2113w | 2010w, 1915 | 1742 |
| *cis*-**6**$^+$ | NC | P(OEt)$_3$ | P(OPh)$_3$ | H | Orange | 70 | 53.2 (53.3) | 4.3 (4.6) | 2.1 (2.1) | — | 2127w | 1958, 1894 | 1763 |
| *trans*-**6**$^+$ | NC | P(OEt)$_3$ | P(OPh)$_3$ | H | Orange | 55 | 53.8 (53.3) | 4.6 (4.6) | 2.2 (2.1) | — | 2124w | 2010w, 1915 | 1764 |
| *cis*-**7**$^+$ | NC | P(OEt)$_3$ | CNBu$^t$ | H | Red | 38 | 50.2 (50.1) | 4.7 (5.0) | 3.7 (3.9) | 2168m | 2133w | 1958, 1894 | 1762 |
| *trans*-**7**$^+$ | NC | P(OEt)$_3$ | CNBu$^t$ | H | Yellow | 73 | 50.4 (50.1) | 4.8 (5.0) | 3.9 (3.9) | 2168m | 2132w | 2010w, 1916 | 1763 |
| *cis*-**8**$^+$ | NC | P(OEt)$_3$ | CNXyl | H | Red | 67 | 51.8 (52.2) | 4.7 (4.7) | 3.3 (3.7) | 2145m | 2132w | 1958, 1894 | 1766 |
| *trans*-**8**$^+$ | NC | P(OEt)$_3$ | CNXyl | H | Orange | 54 | 51.7 (52.2) | 4.6 (4.7) | 3.5 (3.7) | 2146m | 2131w | 2010w, 1916 | 1766 |
| *cis*-**9**$^+$ | NC | P(OPh)$_3$ | CNBu$^t$ | Me | Orange | 72 | 54.8 (54.6)[d] | 4.8 (4.7) | 3.3 (3.1) | 2152m | 2121w | 1970, 1905 | 1742 |
| *trans*-**9**$^+$ | NC | P(OPh)$_3$ | CNBu$^t$ | Me | Orange | 48 | 56.8 (57.2) | 4.7 (4.8) | 2.9 (3.3) | 2154m | 2123w | 2021w, 1931 | 1740 |
| *cis*-**10**$^+$ | NC | P(OEt)$_3$ | CNBu$^t$ | Me | Red | 55 | 51.5 (51.8) | 5.6 (5.4) | 3.6 (3.7) | 2154m | 2118w | 1958, 1894 | 1741 |
| *trans*-**10**$^+$ | NC | P(OEt)$_3$ | CNBu$^t$ | Me | Orange | 30 | 52.1 (51.8) | 5.5 (5.4) | 4.1 (3.7) | 2153m | 2120w | 2009w, 1914 | 1740 |
| *cis*-**11**$^+$ | CN | P(OPh)$_3$ | PPh$_3$ | H | Green | 47 | 59.7 (59.9) | 4.4 (4.2) | 2.3 (2.0) | — | 2104w | 1974, 1920 | 1734 |
| *trans*-**11**$^+$ | CN | P(OPh)$_3$ | PPh$_3$ | H | Green | 31 | 59.8 (59.9) | 4.1 (4.2) | 1.9 (2.0) | — | 2081w | 2016w, 1936 | 1735 |
| *cis*-**12**$^+$ | CN | P(OPh)$_3$ | P(OPh)$_3$ | H | Pink | 56 | 57.9 (58.0) | 3.6 (4.1) | 2.4 (1.9) | — | 2121w | 1973, 1920 | 1756 |
| *trans*-**12**$^+$ | CN | P(OPh)$_3$ | P(OPh)$_3$ | H | Brown | 45 | 58.0 (58.0) | 4.1 (4.1) | 2.2 (1.9) | — | 2103w | 2015w, 1935 | 1756 |
| *cis*-**13**$^+$ | CN | P(OPh)$_3$ | CNBu$^t$ | H | Pink | 81 | 55.7 (55.9) | 4.5 (4.4) | 3.4 (3.4) | 2171m | 2128w | 1975, 1922 | 1758 |
| *trans*-**13**$^+$ | CN | P(OPh)$_3$ | CNBu$^t$ | H | Green | 74 | 56.0 (55.9) | 4.4 (4.4) | 3.4 (3.4) | 2172m | 2111w | 2015w, 1936 | 1757 |
| *cis*-**14**$^+$ | CN | P(OPh)$_3$ | CNXyl | H | Purple | 62 | 57.6 (57.6) | 4.4 (4.2) | 3.3 (3.3) | 2147m | 2132sh | 1974, 1922 | 1761 |
| *trans*-**14**$^+$ | CN | P(OPh)$_3$ | CNXyl | H | Black | 53 | 57.5 (57.6) | 4.1 (4.2) | 3.2 (3.3) | 2147m | 2111w | 2017w, 1936 | 1760 |
| *cis*-**15**$^+$ | CN | P(OEt)$_3$ | PPh$_3$ | H | Green | 44 | 55.1 (55.3) | 4.9 (4.7) | 2.2 (2.2) | — | 2099w | 1963, 1908 | 1736 |
| *trans*-**15**$^+$ | CN | P(OEt)$_3$ | PPh$_3$ | H | Green | 28 | 54.8 (55.3) | 4.4 (4.7) | 2.2 (2.2) | — | 2088w | 2006w, 1921 | 1734 |
| *cis*-**16**$^+$ | CN | P(OEt)$_3$ | P(OPh)$_3$ | H | Red | 44 | 53.2 (53.3) | 4.3 (4.6) | 2.1 (2.1) | — | 2113w | 1962, 1906 | 1758 |
| *trans*-**16**$^+$ | CN | P(OEt)$_3$ | P(OPh)$_3$ | H | Brown | 40 | 53.0 (53.3) | 4.6 (4.6) | 2.3 (2.1) | — | 2096w | 2006w, 1922 | 1757 |
| *cis*-**17**$^+$ | CN | P(OEt)$_3$ | CNBu$^t$ | H | Pink | 70 | 49.6 (50.1) | 5.1 (5.0) | 3.8 (3.9) | 2172m | 2123w | 1962, 1907 | 1758 |
| *trans*-**17**$^+$ | CN | P(OEt)$_3$ | CNBu$^t$ | H | Green | 66 | 50.4 (50.1) | 5.0 (5.0) | 3.8 (3.9) | 2172m | 2106w | 2007w, 1921 | 1757 |
| *cis*-**18**$^+$ | CN | P(OEt)$_3$ | CNXyl | H | Pink | 40 | 51.7 (52.2) | 4.6 (4.7) | 3.5 (3.7) | 2145m | 2128sh | 1962, 1907 | 1761 |
| *trans*-**18**$^+$ | CN | P(OEt)$_3$ | CNXyl | H | Green | 34 | 51.7 (52.2) | 4.7 (4.7) | 3.3 (3.7) | 2146m | 2105w | 2006w, 1921 | 1760 |
| *cis*-**19**$^+$ | CN | P(OPh)$_3$ | CNBu$^t$ | Me | Green | 55 | 57.0 (57.2) | 4.8 (4.8) | 3.0 (3.3) | 2158m | 2114w | 1969, 1903 | 1735 |
| *trans*-**19**$^+$ | CN | P(OPh)$_3$ | CNBu$^t$ | Me | Brown | 56 | 57.4 (57.2) | 4.7 (4.8) | 3.1 (3.3) | 2157m | 2113w | 2015w, 1928 | 1733 |
| *cis*-**20**$^+$ | CN | P(OEt)$_3$ | CNBu$^t$ | Me | Pink | 68 | 51.2 (51.8) | 5.6 (5.4) | 4.1 (3.7) | 2158m | 2113w | 1961, 1906 | 1734 |
| *trans*-**20**$^+$ | CN | P(OEt)$_3$ | CNBu$^t$ | Me | Brown | 45 | 51.4 (51.8) | 5.5 (5.4) | 3.9 (3.7) | 2157m | 2111w | 2004w, 1920 | 1733 |

[a] Isolated as [PF$_6$]$^-$ salts. [b] Calculated values in parentheses. [c] Strong absorptions in $CH_2Cl_2$ unless stated otherwise; sh = shoulder, m = medium, w = weak. [d] Analysed as a 1 : 1 $CH_2Cl_2$ solvate.

**Table 2** Selected bond lengths (Å) and angles (°) for *trans*-[(dppm)(CO)$_2${(EtO)$_3$P}Mn(μ-NC)Mn(CNBu$^t$)(NO)(η$^5$-C$_5$H$_4$Me)]$^+$ *trans*-**7**$^+$ and *trans*-[(dppm)(CO)$_2${(EtO)$_3$P}Mn(μ-CN)Mn(CNBu$^t$)(NO)(η$^5$-C$_5$H$_4$Me)]$^+$ *trans*-**17**$^+$

| | *trans*-**7**$^+$ | *trans*-**17**$^+$ | | *trans*-**7**$^+$ | *trans*-**17**$^+$ |
|---|---|---|---|---|---|
| Mn(1)–C(1) | 1.951(3) | — | Mn(1)–C(1)–N(1) | 176.9(3) | — |
| Mn(1)–N(1) | — | 1.968(3) | Mn(1)–N(1)–C(1) | — | 173.6(2) |
| Mn(2)–N(1) | 2.010(3) | — | Mn(2)–N(1)–C(1) | 171.6(2) | — |
| Mn(2)–C(1) | — | 1.955(3) | Mn(2)–C(1)–N(1) | — | 175.0(2) |
| C(1)–N(1) | 1.153(4) | 1.151(4) | N(1)–Mn(1)–C(1) | 96.3(2) | — |
| Mn(1)–N(2) | 1.656(3) | 1.655(3) | N(1)–Mn(1)–N(2) | — | 98.3(1) |
| Mn(1)–C(8) | 1.916(4) | 1.922(3) | C(1)–Mn(1)–C(8) | 88.6(1) | — |
| N(2)–O(1) | 1.171(4) | 1.176(3) | C(8)–Mn(1)–N(1) | — | 89.4(1) |
| C(8)–N(3) | 1.150(4) | 1.151(4) | Mn(1)–N(2)–O(1) | 175.9(3) | 174.4(3) |
| Mn(2)–P(1) | 2.296(1) | 2.283(9) | C(8)–Mn(1)–N(2) | 96.1(2) | 95.8(1) |
| Mn(2)–P(2) | 2.275(1) | 2.290(9) | P(1)–Mn(2)–P(2) | 72.5(1) | 72.2 (3) |
| Mn(2)–P(3) | 2.211(1) | 2.205(10) | P(2)–Mn(2)–P(3) | 100.4(1) | 100.8(3) |
| Mn(2)–C(14) | 1.839(3) | 1.829(3) | P(1)–Mn(2)–P(3) | 172.8(1) | 172.9(4) |
| Mn(2)–C(13) | 1.834(3) | 1.827(3) | N(1)–Mn(2)–P(2) | 165.3(1) | — |
| C(14)–O(3) | 1.146(4) | 1.147(3) | C(1)–Mn(2)–P(2) | — | 164.8(8) |
| C(13)–O(2) | 1.147(4) | 1.149(3) | C(14)–Mn(2)–C(13) | 178.7(1) | 176.5(1) |
| | | | Mn(2)–C(14)–O(3) | 177.3(3) | 176.6(3) |
| Mn(1)···Mn(2) | 5.096 | 5.058 | Mn(2)–C(13)–O(2) | 179.1(3) | 179.7(3) |

**Table 3** Selected bond lengths (Å) and angles (°) for *cis*-[(dppm)(CO)$_2${(PhO)$_3$P}Mn(μ-NC)Mn{P(OPh)$_3$}(NO)(η$^5$-C$_5$H$_4$Me)]$^+$ *cis*-**2**$^+$ and *cis*-[(dppm)(CO)$_2${(PhO)$_3$P}Mn(μ-CN)Mn{P(OPh)$_3$}(NO)(η$^5$-C$_5$H$_4$Me)]$^+$ *cis*-**12**$^+$

| | *cis*-**2**$^+$ | *cis*-**12**$^+$ [a] | | *cis*-**2**$^+$ | *cis*-**12**$^+$ [a] |
|---|---|---|---|---|---|
| Mn(1)–C(1) | — | 1.960(8) | Mn(1)–C(1)–N(1) | — | 178.7(6) |
| Mn(1)′–C(1)′ | — | 1.994(7) | Mn(1)′–C(1)′–N(1)′ | — | 179.0(6) |
| Mn(1)–N(1) | 2.033(14) | — | Mn(1)–N(1)–C(1) | 175.8(13) | — |
| Mn(2)–N(1) | — | 1.927(6) | Mn(2)–N(1)–C(1) | — | 173.4(6) |
| Mn(2)′–N(1)′ | — | 1.935(6) | Mn(2)′–N(1)′–C(1)′ | — | 176.7(6) |
| Mn(2)–C(1) | 1.912(17) | — | Mn(2)–C(1)–N(1) | 171.1(15) | — |
| C(1)–N(1) | 1.184(16) | 1.180(7) | P(4)–Mn(2)–N(1) | — | 86.06(17) |
| C(1)′–N(1)′ | — | 1.147(7) | P(4)′–Mn(2)′–N(1)′ | — | 86.16(15) |
| Mn(2)–N(2) | 1.637(17) | 1.612(8) | P(4)–Mn(2)–C(1) | 87.9(5) | — |
| Mn(2)′–N(2)′ | — | 1.631(7) | | | |
| Mn(2)–P(4) | 2.198(6) | 2.218(2) | N(2)–Mn(2)–N(1) | — | 98.9(3) |
| Mn(2)′–P(4)′ | — | 2.204(2) | N(2)′–Mn(2)′–N(1)′ | — | 100.6(3) |
| N(2)–O(1) | 1.218(17) | 1.210(8) | N(2)–Mn(2)–C(1) | 96.6(7) | — |
| N(2)′–O(1)′ | — | 1.192(7) | | | |
| Mn(1)–P(1) | 2.285(6) | 2.324(2) | C(1)–Mn(1)–P(2) | — | 86.38(19) |
| Mn(1)′–P(1)′ | — | 2.348(2) | C(1)′–Mn(1)′–P(2)′ | — | 87.54(18) |
| Mn(1)–P(2) | 2.340(6) | 2.293(2) | N(1)–Mn(1)–P(2) | 88.2(4) | — |
| Mn(1)′–P(2)′ | — | 2.285(2) | | | |
| Mn(1)–P(3) | 2.207(6) | 2.197(2) | Mn(2)–N(2)–O(1) | 172.7(14) | 171.1(6) |
| Mn(1)′–P(3)′ | — | 2.208(2) | Mn(2)′–N(2)′–O(1)′ | — | 173.7(6) |
| Mn(1)–C(2) | 1.753(19) | 1.795(8) | P(4)–Mn(2)–N(2) | 94.2(5) | 98.6(2) |
| Mn(1)′–C(2)′ | — | 1.814(7) | P(4)′–Mn(2)′–N(2)′ | — | 95.0(2) |
| Mn(1)–C(3) | 1.727(17) | 1.798(7) | P(1)–Mn(1)–P(2) | 72.9(2) | 72.35(7) |
| Mn(1)′–C(3)′ | — | 1.785(7) | P(1)′–Mn(1)′–P(2)′ | — | 72.41(7) |
| C(2)–O(2) | 1.197(18) | 1.133(7) | P(2)–Mn(1)–P(3) | 96.1(2) | 167.05(8) |
| C(2)′–O(2)′ | — | 1.170(7) | P(2)′–Mn(1)′–P(3)′ | — | 171.48(8) |
| C(3)–O(3) | 1.199(16) | 1.154(7) | P(1)–Mn(1)–P(3) | 168.7(2) | 94.94(8) |
| C(3)′–O(3)′ | — | 1.161(7) | P(1)′–Mn(1)′–P(3)′ | — | 99.42(8) |
| | | | C(2)–Mn(1)–C(3) | 86.8(8) | 89.7(3) |
| | | | C(2)′–Mn(1)′–C(3)′ | — | 88.3(3) |
| Mn(1)…Mn(2) | 5.109 | 5.059 | Mn(1)–C(2)–O(2) | 175.3(17) | 177.9(7) |
| Mn(1)′…Mn(2)′ | — | 5.073 | Mn(1)′–C(2)′–O(2)′ | — | 174.2(6) |
| | | | Mn(1)–C(3)–O(3) | 175.5(14) | 175.6(5) |
| | | | Mn(1)′–C(3)′–O(3)′ | — | 178.1(6) |

[a] There are two independent molecules in the asymmetric unit. Equivalent atoms for the second are distinguished from the first by primes.

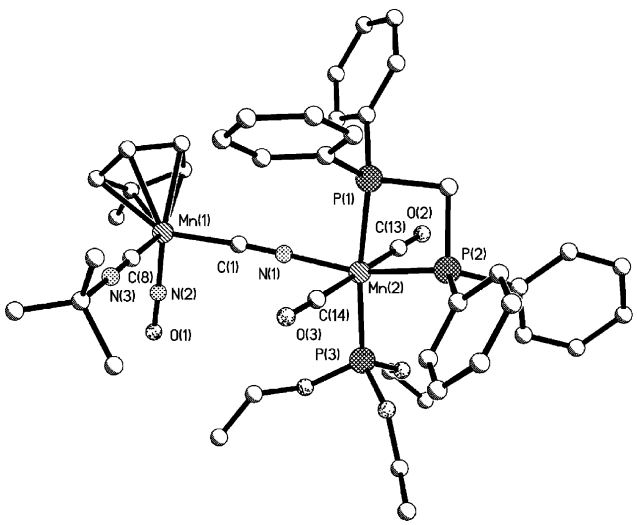


**Fig. 1** The structure of *trans*-[(dppm)(CO)$_2${(EtO)$_3$P}Mn(μ-CN)Mn(CNBu$^t$)(NO)(η$^5$-C$_5$H$_4$Me)]$^+$ *trans*-**17**$^+$. The hydrogen atoms have been omitted for clarity.

The μ-CN bond lengths are in the range 1.15–1.18 Å, similar to those in other cyanide-bridged complexes.[12]

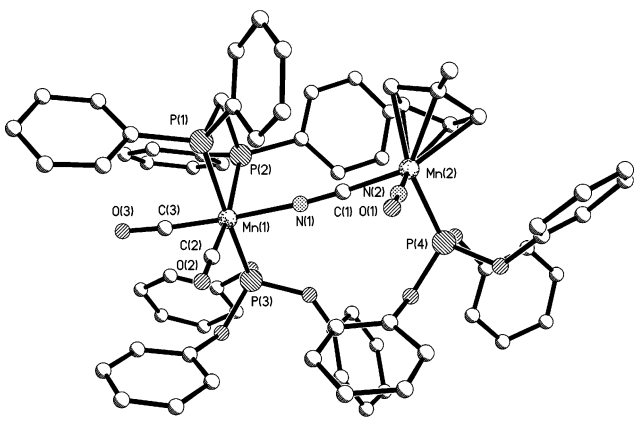


**Fig. 2** The structure of *cis*-[(dppm)(CO)$_2${(PhO)$_3$P}Mn(μ-NC)Mn{P(OPh)$_3$}(NO)(η$^5$-C$_5$H$_4$Me)]$^+$ *cis*-**2**$^+$. Hydrogen atoms have been omitted for clarity.

As found in the other structurally characterised linkage isomers noted above,[10,11] the molecular structures of *trans*-**7**$^+$ and *trans*-**17**$^+$ are very similar. (They are crystallographically isostructural.) By contrast, those of *cis*-**2**$^+$ and *cis*-**12**$^+$ are rather different, at least in the solid state. Thus, the torsion angle, τ, formed by the two Mn–P(OPh)$_3$ vectors (*i.e.* P–Mn–XY–Mn–P with the

 

**Table 4** Selected bond lengths (Å) and angles (°) for *cis*-[(dppm)(CO)$_2${(EtO)$_3$P}Mn(μ-NC)Mn(CNXyl)(NO)(η$^5$-C$_5$H$_4$Me)]$^+$ *cis*-**8**$^+$ and *cis*-[(dppm)(CO)$_2${(PhO)$_3$P}Mn(μ-NC)Mn(CNBu$^t$)(NO)(η$^5$-C$_5$Me$_5$)]$^+$ *cis*-**9**$^+$

| | *cis*-**8**$^+$ | *cis*-**9**$^+$ | | *cis*-**8**$^+$ | *cis*-**9**$^+$ |
|---|---|---|---|---|---|
| Mn(1)–C(1) | 1.951(5) | 1.938(9) | Mn(1)–C(1)–N(1) | 177.0(5) | 176.6(7) |
| Mn(2)–N(1) | 2.012(4) | 1.996(7) | Mn(2)–N(1)–C(1) | 176.3(4) | 176.0(6) |
| C(1)–N(1) | 1.157(5) | 1.161(9) | Mn(1)–N(2)–O(2) | 176.5(4) | 173.8(10) |
| Mn(1)–N(2) | 1.653(5) | 1.629(10) | C(42)–Mn(1)–N(2) | 96.2(2) | 97.2(5) |
| Mn(1)–C(42) | 1.892(6) | 1.883(10) | N(2)–Mn(1)–C(1) | 96.2(2) | 99.7(4) |
| N(2)–O(1) | 1.182(5) | 1.179(12) | C(42)–Mn(1)–C(1) | 91.5(2) | 90.5(3) |
| C(42)–N(3) | 1.158(6) | 1.150(10) | P(1)–Mn(2)–P(2) | 72.3(1) | 70.7(1) |
| Mn(2)–P(1) | 2.298(2) | 2.303(2) | P(2)–Mn(2)–P(3) | 98.9(1) | 97.7(1) |
| Mn(2)–P(2) | 2.358(2) | 2.352(2) | P(3)–Mn(2)–P(1) | 170.9(1) | 168.0(1) |
| Mn(2)–P(3) | 2.224(2) | 2.202(3) | N(1)–Mn(2)–P(2) | 84.8(1) | 84.8(2) |
| Mn(2)–C(2) | 1.806(8) | 1.791(9) | C(2)–Mn(2)–C(3) | 89.8(2) | 88.7(4) |
| Mn(2)–C(3) | 1.777(5) | 1.742(9) | Mn(2)–C(2)–O(2) | 177.8(5) | 174.9(7) |
| C(2)–O(2) | 1.159(7) | 1.153(9) | Mn(2)–C(3)–O(3) | 178.8(5) | 176.2(1) |
| C(3)–O(3) | 1.162(5) | 1.164(10) | | | |
| Mn(1)...Mn(2) | 5.114 | 5.086 | | | |

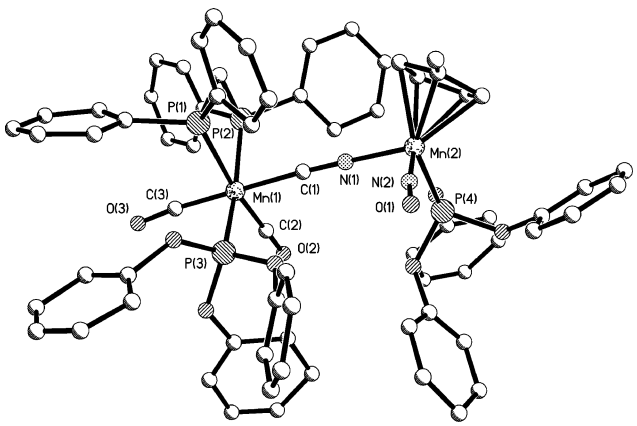


**Fig. 3** The structure of *cis*-[(dppm)(CO)$_2${(PhO)$_3$P}Mn(μ-CN)Mn{P(OPh)$_3$}(NO)(η$^5$-C$_5$H$_4$Me)]$^+$ *cis*-**12**$^+$. Hydrogen atoms have been omitted for clarity.

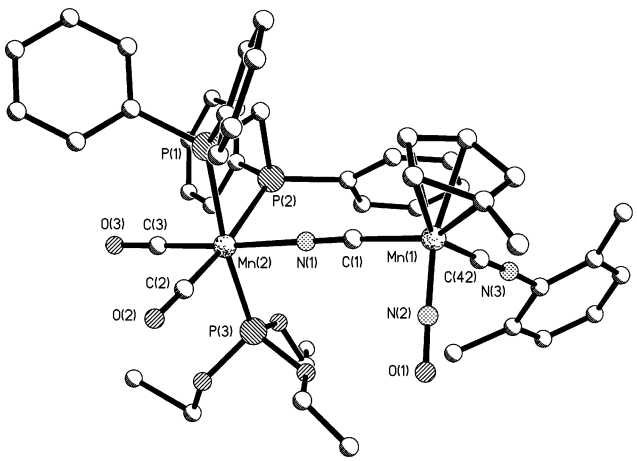


**Fig. 4** The structure of *cis*-[(dppm)(CO)$_2${(EtO)$_3$P}Mn(μ-NC)Mn(CNXyl)(NO)(η$^5$-C$_5$H$_4$Me)]$^+$ *cis*-**8**$^+$. Hydrogen atoms have been omitted for clarity.

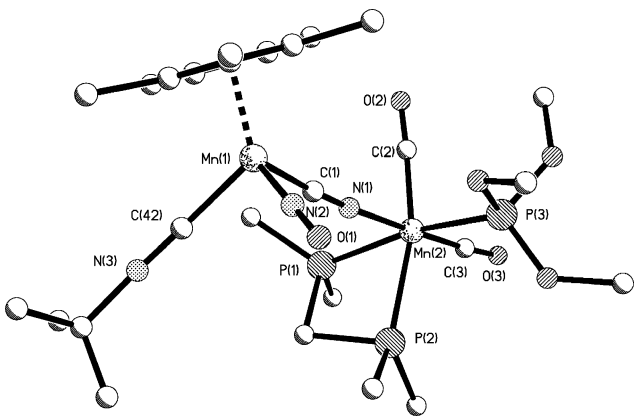


**Fig. 5** The structure of *cis*-[(dppm)(CO)$_2${(PhO)$_3$P}Mn(μ-NC)Mn(CNBu$^t$)(NO)(η$^5$-C$_5$Me$_5$)]$^+$ *cis*-**9**$^+$. Hydrogen atoms and all but the *ipso* carbons of the phenyl rings of dppm have been omitted for clarity.

Mn–XY–Mn backbone assumed to be linear) is 13.2° for *cis*-**2**$^+$ and 86.1 and 76.2° for the two independent units of *cis*-**12**$^+$ respectively. Formally, this appears to be the result of *N*- and *C*-coordination respectively of two different optical isomers of the *pseudo*-tetrahedral units (NC)Mn{P(OPh)$_3$}(NO)(η$^5$-C$_5$H$_4$Me) and (CN)Mn{P(OPh)$_3$}(NO)(η$^5$-C$_5$H$_4$Me) to the octahedral manganese centre, *i.e.* *cis*-**2**$^+$ and *cis*-**12**$^+$ are different diastereoisomers. (Each of *cis*-**1**$^+$ to *cis*-**20**$^+$ can exist as diastereoisomers although in no case has evidence been found for the co-existence of two such isomers, *e.g.* by IR spectroscopy.)

The structural analysis of *cis*-**9**$^+$ is the first of a complex containing the *N*-donor cyanomanganese ligand [Mn(CN)(CNBu$^t$)(NO)(η$^5$-C$_5$Me$_5$)] the estimated cone angle of which, $\theta$, (106°) is larger than that of [Mn(CN)(CNBu$^t$)(NO)(η$^5$-C$_5$H$_4$Me)] ($\theta$ = 57°) due to the increased methylation on the cyclopentadienyl ring. Thus, the structure of *cis*-**9**$^+$ differs from those of the other *cis* complexes, *cis*-**2**$^+$, *cis*-**8**$^+$ and *cis*-**12**$^+$, in the relative arrangement of the metal fragments. In the less sterically hindered complexes, such as *cis*-**8**$^+$, the η$^5$-C$_5$H$_4$Me ring and the dppm ligand are *syn* relative to each other (Fig. 4). However, in complex *cis*-**9**$^+$ the bulky η$^5$-C$_5$Me$_5$ and dppm ligands are positioned *anti* to each other (Fig. 5).

## Electrochemical studies

The cyclic voltammograms (CVs) of **1**$^+$–**20**$^+$ each show two oxidation waves (Table 5) in $CH_2Cl_2$ at a platinum electrode,

**Table 5** Electrochemical data[a] for *cis*- and *trans*-[(dppm)$(CO)_2$LMn(μ-XY)MnL′$(NO)(\eta^5$-$C_5R_4Me)][PF_6]$

| | | | | | Process ($E^{\circ\prime}$/V)[b] | | |
|---|---|---|---|---|---|---|---|
| Complex | L | L′ | R | XY | + → 2+ | 2+ → 3+ | $\Delta E^{\circ\prime}$[c]/V |
| *cis*-**1**$^+$ | $P(OPh)_3$ | $PPh_3$ | H | NC | 1.03 | 1.54(I) (0.70, 1.36)[d] | — |
| *trans*-**1**$^+$ | $P(OPh)_3$ | $PPh_3$ | H | NC | 0.68 | 1.35 | 0.67 |
| *cis*-**2**$^+$ | $P(OPh)_3$ | $P(OPh)_3$ | H | NC | 1.24(I) (0.73) | (1.60) | — |
| *trans*-**2**$^+$ | $P(OPh)_3$ | $P(OPh)_3$ | H | NC | 0.73 | 1.61 | 0.88 |
| *cis*-**3**$^+$ | $P(OPh)_3$ | $CNBu^t$ | H | NC | 1.20(I) (0.73) | (1.43) | — |
| *trans*-**3**$^+$ | $P(OPh)_3$ | $CNBu^t$ | H | NC | 0.72 | 1.45 | 0.73 |
| *cis*-**4**$^+$ | $P(OPh)_3$ | CNXyl | H | NC | 1.26(I) (0.72) | (1.51) | — |
| *trans*-**4**$^+$ | $P(OPh)_3$ | CNXyl | H | NC | 0.74 | 1.47 | 0.73 |
| *cis*-**5**$^+$ | $P(OEt)_3$ | $PPh_3$ | H | NC | 1.02(I) (0.54) | (1.34) | — |
| *trans*-**5**$^+$ | $P(OEt)_3$ | $PPh_3$ | H | NC | 0.53 | 1.31 | 0.78 |
| *cis*-**6**$^+$ | $P(OEt)_3$ | $P(OPh)_3$ | H | NC | 1.09(I) (0.55) | (1.56) | — |
| *trans*-**6**$^+$ | $P(OEt)_3$ | $P(OPh)_3$ | H | NC | 0.57 | 1.55 | 0.98 |
| *cis*-**7**$^+$ | $P(OEt)_3$ | $CNBu^t$ | H | NC | 1.06(I) (0.54) | (1.36) | — |
| *trans*-**7**$^+$ | $P(OEt)_3$ | $CNBu^t$ | H | NC | 0.55 | 1.36 | 0.81 |
| *cis*-**8**$^+$ | $P(OEt)_3$ | CNXyl | H | NC | 1.11(I) (0.56) | (1.44) | — |
| *trans*-**8**$^+$ | $P(OEt)_3$ | CNXyl | H | NC | 0.55 | 1.43 | 0.88 |
| *cis*-**9**$^+$ | $P(OPh)_3$ | $CNBu^t$ | Me | NC | 0.99 | 1.51(I) (0.64, 1.25)[d] | — |
| *trans*-**9**$^+$ | $P(OPh)_3$ | $CNBu^t$ | Me | NC | 0.67 | 1.28 | 0.61 |
| *cis*-**10**$^+$ | $P(OEt)_3$ | $CNBu^t$ | Me | NC | 0.99(I) (0.50) | (1.30) | — |
| *trans*-**10**$^+$ | $P(OEt)_3$ | $CNBu^t$ | Me | NC | 0.51 | 1.32 | 0.81 |
| *cis*-**11**$^+$ | $P(OPh)_3$ | $PPh_3$ | H | CN | 0.84 | 1.65(I) (1.28) | — |
| *trans*-**11**$^+$ | $P(OPh)_3$ | $PPh_3$ | H | CN | 0.76 | 1.31 | 0.55 |
| *cis*-**12**$^+$ | $P(OPh)_3$ | $P(OPh)_3$ | H | CN | 1.08 | 1.65(I) (1.40) | — |
| *trans*-**12**$^+$ | $P(OPh)_3$ | $P(OPh)_3$ | H | CN | 0.90 | 1.42 | 0.52 |
| *cis*-**13**$^+$ | $P(OPh)_3$ | $CNBu^t$ | H | CN | 1.01 | 1.58(I) (1.39) | — |
| *trans*-**13**$^+$ | $P(OPh)_3$ | $CNBu^t$ | H | CN | 0.87 | 1.28 | 0.41 |
| *cis*-**14**$^+$ | $P(OPh)_3$ | CNXyl | H | CN | 1.07 | 1.56(I) (1.39) | — |
| *trans*-**14**$^+$ | $P(OPh)_3$ | CNXyl | H | CN | 0.92 | 1.33 | 0.41 |
| *cis*-**15**$^+$ | $P(OEt)_3$ | $PPh_3$ | H | CN | 0.79 | 1.44(I) (1.22) | — |
| *trans*-**15**$^+$ | $P(OEt)_3$ | $PPh_3$ | H | CN | 0.69 | 1.19 | 0.50 |
| *cis*-**16**$^+$ | $P(OEt)_3$ | $P(OPh)_3$ | H | CN | 1.06(I) (0.73) | 1.42 | — |
| *trans*-**16**$^+$ | $P(OEt)_3$ | $P(OPh)_3$ | H | CN | 0.77 | 1.36 | 0.59 |
| *cis*-**17**$^+$ | $P(OEt)_3$ | $CNBu^t$ | H | CN | 0.98 (0.72) | 1.39(I) (1.21) | — |
| *trans*-**17**$^+$ | $P(OEt)_3$ | $CNBu^t$ | H | CN | 0.72 | 1.21 | 0.49 |
| *cis*-**18**$^+$ | $P(OEt)_3$ | CNXyl | H | CN | 1.05(I) (0.74) | 1.31 | — |
| *trans*-**18**$^+$ | $P(OEt)_3$ | CNXyl | H | CN | 0.75 | 1.31 | 0.56 |
| *cis*-**19**$^+$ | $P(OPh)_3$ | $CNBu^t$ | Me | CN | 0.75 | 1.57(I) (1.34) | — |
| *trans*-**19**$^+$ | $P(OPh)_3$ | $CNBu^t$ | Me | CN | 0.88 | 1.20 | 0.32 |
| *cis*-**20**$^+$ | $P(OEt)_3$ | $CNBu^t$ | Me | CN | 0.78 | 1.41(I) (1.21) | — |
| *trans*-**20**$^+$ | $P(OEt)_3$ | $CNBu^t$ | Me | CN | 0.70 | 1.18 | 0.48 |

[a] At a Pt electrode in $CH_2Cl_2$, with potentials relative to the saturated calomel electrode, calibrated *vs.* the $[Fe(\eta\text{-}C_5Me_5)_2]^+/[Fe(\eta\text{-}C_5Me_5)_2]$ couple (at −0.08 V). [b] For an irreversible (I) process, the oxidation peak potential, $(E_p)_{ox}$, is given at a scan rate of 200 mV $s^{-1}$. Potentials for associated reversible product waves are given in parentheses. [c] $\Delta E^{\circ\prime}$ is the difference between the potentials for the two reversible oxidation waves (of the *trans*$^+$ isomers only). [d] The two product waves, observed only after scanning the second, irreversible, oxidation wave, are due to the *trans*-dication/*trans*-monocation and *trans*-trication/*trans*-dication couples respectively.

corresponding to the sequential oxidation of the two metal centres. Generally, the waves are reversible on the cyclic voltammetry timescale when the coordination geometry of the manganese centre is *pseudo*-tetrahedral or *trans*-dicarbonyl octahedral. However, they are irreversible when a *cis*-dicarbonyl unit is oxidised due to the redox-induced *cis–trans* isomerisation of the $Mn^{II}(CO)_2$ fragment.[5] In these cases, the irreversible oxidation wave is coupled to a reversible product wave, at a more negative potential.

The occurrence of an irreversible oxidation wave for *cis*-[(dppm)$(CO)_2$LMn(μ-XY)Mn$(NO)$L′$(\eta^5$-$C_5R_4Me)]^+$ therefore allows the identification of which manganese centre is oxidised first (aided by comparing the individual redox potentials with those of the corresponding mononuclear units and noting the effects of altering the ligands L and L′ or the extent of ring methylation in $\eta^5$-$C_5R_4Me$). As noted previously,[3] increased ring methylation in $[Mn(CN)(CNBu^t)(NO)(\eta^5\text{-}C_5R_4Me)]$, from $\eta^5$-$C_5H_4Me$ to $\eta^5$-$C_5Me_5$, lowers the oxidation potential by 210 mV; better donors L and L′ shift oxidation waves to less positive potentials, *e.g.* the oxidation potential of $[Mn(CN)L'(NO)(\eta^5\text{-}C_5H_4Me)]$ decreases from 1.11 V (L′ = CNXyl) to 0.85 V (L′ = $PPh_3$) and that of *trans*-$[Mn(CN)L(CO)_2(dppm)]$ decreases from 0.64 V {L = $P(OPh)_3$} to 0.50 V {L = $P(OEt)_3$}.

The variation of the orientation of the cyanide bridge, of the ligands L and L′, of the extent of ring methylation in the $\eta^5$-$C_5R_4Me$ group, and the *cis* or *trans* orientation of the $Mn(CO)_2$ fragment all affect the order in which the metal centres in *cis*-[(dppm)$(CO)_2$LMn(μ-XY)Mn$(NO)$L′$(\eta^5$-$C_5R_4Me)]^+$ are oxidised. This, in turn, leads to control of the direction and energy of metal–metal charge-transfer in the corresponding dications (see below).

The CV of *cis*-[(dppm)$(CO)_2${$(EtO)_3P$}Mn(μ-NC)Mn-{$P(OPh)_3$}$(NO)(\eta^5$-$C_5H_4Me)]^+$ *cis*-**6**$^+$ [Fig. 6(a)] shows one irreversible oxidation wave at 1.09 V followed by a reversible

 

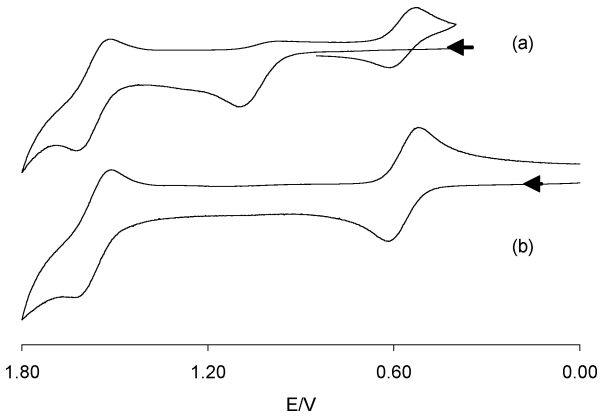


**Fig. 6** The CVs in $CH_2Cl_2$ of (a) *cis*-[(dppm)$(CO)_2${$(EtO)_3P$}Mn(μ-NC)Mn{$P(OPh)_3$}$(NO)(\eta^5$-$C_5H_4Me)]^+$, *cis*-**6**$^+$, from 0.30 to 1.80 to 0.40 to 0.85 V, and (b) *trans*-[(dppm)$(CO)_2${$(EtO)_3P$}Mn(μ-NC)Mn{$P(OPh)_3$}-$(NO)(\eta^5$-$C_5H_4Me)]^+$, *trans*-**6**$^+$, from 0.0 to 1.80 V at a scan rate of 200 mV $s^{-1}$.

product oxidation wave at 1.56 V, and a product reduction wave, at 0.52 V, which a subsequent scan shows to be reversible and centred at 0.55 V. Thus, the first step is oxidation at the *cis*-$Mn(CO)_2$ site; the two product waves appear at potentials identical to those of *trans*-**6**$^+$ [Fig. 6(b)], confirming that after oxidation at the *N*-bound *cis*-$Mn(CO)_2$ unit, *cis*-**6**$^{2+}$ rapidly isomerises to *trans*-**6**$^{2+}$.

The CV of *cis*-[(dppm)$(CO)_2${$(PhO)_3P$}Mn(μ-NC)Mn{P-$(OPh)_3$}$(NO)(\eta^5$-$C_5H_4Me)]^+$ *cis*-**2**$^+$ [Fig. 7(a)] is very similar to that of *cis*-**6**$^+$, showing one irreversible process at 1.24 V {oxidation at the *cis*-$Mn(CO)_2$ site}, and two reversible product waves at 1.60 and 0.73 V corresponding to the *trans*-**2**$^{3+}$/*trans*-**2**$^{2+}$ and *trans*-**2**$^{2+}$/*trans*-**2**$^+$ couples for the product of

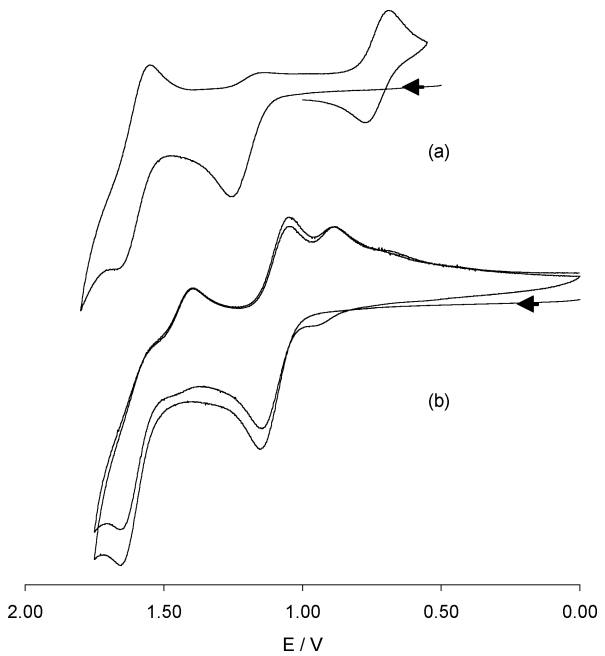


**Fig. 7** The CVs in $CH_2Cl_2$ of *cis*-[(dppm)$(CO)_2${$(PhO)_3P$}-Mn(μ-XY)Mn{$P(OPh)_3$}$(NO)(\eta^5$-$C_5H_4Me)]^+$ (a) XY = NC, *cis*-**2**$^+$, from 0.50 to 1.80 to 0.50 to 0.90 V, and (b) XY = CN, *cis*-**12**$^+$, from 0.0 to 1.80 V, multiple scan, at a scan rate of 200 mV $s^{-1}$.

oxidative isomerisation. However, the CV of its linkage isomer *cis*-[(dppm)$(CO)_2${$(PhO)_3P$}Mn(μ-CN)Mn{$P(OPh)_3$}$(NO)(\eta^5$-$C_5H_4Me)]^+$ *cis*-**12**$^+$ [Fig. 7(b)] shows the first process to be reversible and therefore related to the oxidation of $Mn_{tet}$. The second oxidation process is irreversible with associated product waves identical to those of *trans*-**12**$^+$. Changing the orientation of the cyanide bridge from $Mn_{oct}$–NC–$Mn_{tet}$ (in *cis*-**2**$^+$) to $Mn_{oct}$–CN–$Mn_{tet}$ in (*cis*-**12**$^+$) therefore reverses the order in which the metal centres oxidise. The overall electrochemical behaviour of *cis*-**2**$^+$ and *cis*-**12**$^+$ is summarised in Schemes 3 and 4 respectively.

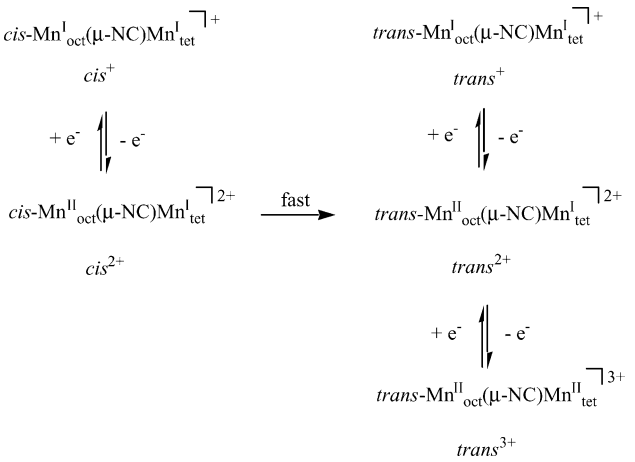


**Scheme 3** The oxidation of *cis*-[(dppm)$(CO)_2${$(PhO)_3P$}Mn(μ-NC)-MnL$(NO)(\eta^5$-$C_5H_4Me)]^+$ {L = $P(OPh)_3$, *cis*-**2**$^+$ or $CNBu^t$, *cis*-**3**$^+$}.

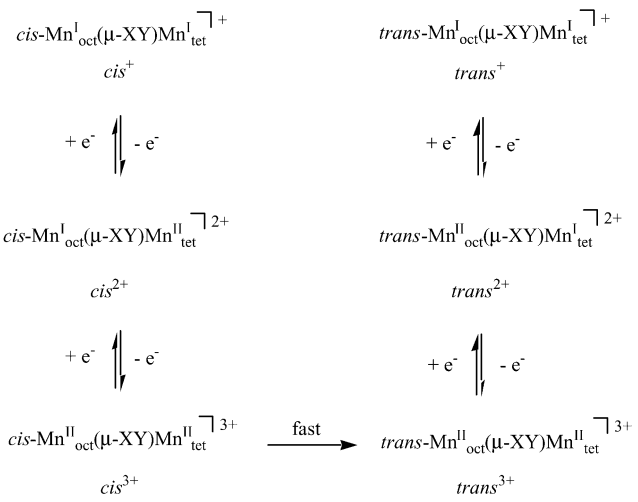


**Scheme 4** The oxidation of *cis*-[(dppm)$(CO)_2${$(PhO)_3P$}Mn(μ-XY)-MnL$(NO)(\eta^5$-$C_5R_4Me)]^+$ {XY = NC, L = $CNBu^t$, R = Me, *cis*-**9**$^+$; XY = CN, L = $P(OPh)_3$, R = H, *cis*-**12**$^+$}.

Complexes [(dppm)$(CO)_2${$(PhO)_3P$}Mn(μ-CN)Mn{$P(OPh)_3$}-$(NO)(\eta^5$-$C_5H_4Me)]^+$ *cis*-**12**$^+$ and *cis*-[(dppm)$(CO)_2${$(EtO)_3P$}Mn-(μ-CN)Mn{$P(OPh)_3$}$(NO)(\eta^5$-$C_5H_4Me)]^+$ *cis*-**16**$^+$ provide an example of the effect of varying L, the ligand at *cis*-$Mn_{oct}$. Although they differ only in the replacement of L = $P(OPh)_3$ in *cis*-**12**$^+$ by L = $P(OEt)_3$ in *cis*-**16**$^+$ their electrochemistry is very different. The CV of *cis*-**16**$^+$ (Fig. 8) shows an irreversible oxidation wave at 1.06 V, corresponding to the oxidation of the octahedral metal centre, and

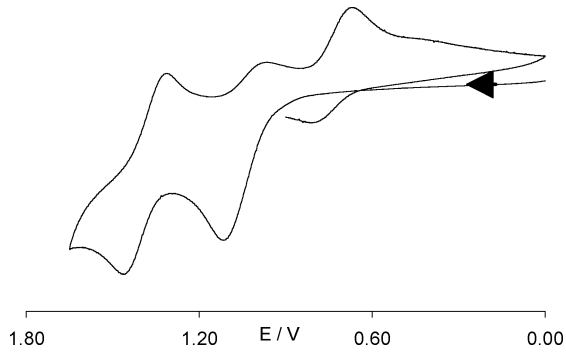


**Fig. 8** The CV in $CH_2Cl_2$ of *cis*-[(dppm)$(CO)_2${$(EtO)_3P$}Mn-(μ-CN)Mn{$P(OPh)_3$}$(NO)(\eta^5$-$C_5H_4Me)]^+$ *cis*-**16**$^+$ from 0.0 to 1.65 to 0.0 to 0.90 V at a scan rate of 200 mV $s^{-1}$.

two product waves at 1.42 and 0.73 V, identical to those of *trans*-**16**$^+$. Thus, changing the phosphite, L, to a better donor leads to the site of first oxidation changing from $Mn_{tet}$ (first oxidation wave reversible) to *cis*-$Mn_{oct}$ (first oxidation wave irreversible).

By contrast, the complexes *cis*-[(dppm)$(CO)_2${$(PhO)_3P$}Mn-(μ-NC)Mn$(PPh_3)(NO)(\eta^5$-$C_5H_4Me)]^+$ *cis*-**1**$^+$ and *cis*-[(dppm)-$(CO)_2${$(PhO)_3P$}Mn(μ-NC)Mn{$P(OPh)_3$}$(NO)(\eta^5$-$C_5H_4Me)]^+$ *cis*-**2**$^+$ provide an example of how the ligand L′ at $Mn_{tet}$ influences the order of oxidation. In the CV of *cis*-**1**$^+$ [Fig. 9(a)] the first wave is reversible and therefore associated with oxidation at $Mn_{tet}$. However, on changing $PPh_3$ (in *cis*-**1**$^+$) for the better π-acceptor $P(OPh)_3$ (in *cis*-**2**$^+$) the first wave becomes irreversible [Fig. 9(b)] indicating oxidation at *cis*-$Mn_{oct}$.

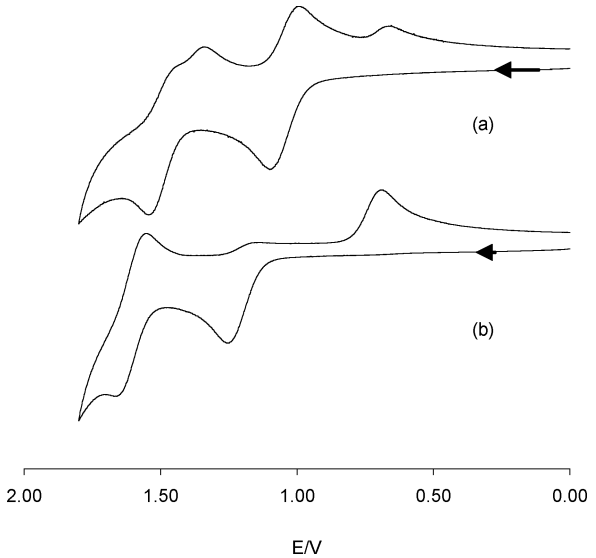


**Fig. 9** The CVs in $CH_2Cl_2$ of *cis*-[(dppm)$(CO)_2${$(PhO)_3P$}Mn-(μ-NC)MnL′$(NO)(\eta^5$-$C_5H_4Me)]^+$ (a) L′ = $PPh_3$, *cis*-**1**$^+$, and (b) L′ = $P(OPh)_3$, *cis*-**2**$^+$ from 0.0 to 1.8 V.

Finally, *cis*-[(dppm)$(CO)_2${$(PhO)_3P$}Mn(μ-NC)Mn$(CNBu^t)$-$(NO)(\eta^5$-$C_5H_4Me)]^+$ *cis*-**3**$^+$ and *cis*-[(dppm)$(CO)_2${$(PhO)_3P$}Mn(μ-NC)Mn$(CNBu^t)(NO)(\eta^5$-$C_5Me_5)]^+$ *cis*-**9**$^+$ show how the extent of methylation of the $\eta^5$-$C_5R_4Me$ group influences the order in which the metal centres are oxidised. The first wave in the CV of *cis*-**3**$^+$ is irreversible and therefore associated with the oxidation of *cis*-$Mn_{oct}$; the two reversible product waves correspond to the *trans*-**3**$^{3+}$/*trans*-**3**$^{2+}$ and *trans*-**3**$^{2+}$/*trans*-**3**$^+$ couples. However, the increased ring methylation in the $\eta^5$-$C_5Me_5$ complex *cis*-**9**$^+$ increases the electron density at $Mn_{tet}$ which is then the first oxidation site; the first oxidation wave is reversible and the second irreversible (oxidation at *cis*-$Mn_{oct}$). The electrochemical behaviour of *cis*-**3**$^+$ is described by Scheme 3 and that of *cis*-**9**$^+$ by Scheme 4.

In the absence of redox-induced isomerisation, the order of oxidation of the two metal centres in *trans*-**1**$^+$–**20**$^+$ can only be assigned by comparing the potentials for the two reversible oxidation waves with those of mononuclear precursors (and related complexes) and by observing the shifts in each oxidation wave as the ligands on each centre are altered.

The first oxidation of *trans*-[(dppm)$(CO)_2${$(EtO)_3P$}Mn(μ-NC)Mn$(CNBu^t)(NO)(\eta^5$-$C_5H_4Me)]^+$ *trans*-**7**$^+$ occurs at 0.55 V. Since the oxidation potential of the mononuclear cyanomanganese ligand [Mn(CN)$(CNBu^t)(NO)(\eta^5$-$C_5H_4Me)]$ occurs at *ca.* 1.0 V, and the potential will increase when this ligand is *N*-coordinated to a second metal, the process at 0.55 V must be related to the oxidation of *trans*-$Mn_{oct}$ in *trans*-**7**$^+$. The second wave, associated with the oxidation of $Mn_{tet}$, is centred at 1.36 V which compares well with that of the mononuclear complex $[Mn(CNBu^t)_2(NO)(\eta^5$-$C_5H_4Me)]^+$ ($E^{o\prime}$ = 1.45 V).[3] (In this case, the assignment of the order of oxidation for *trans*-**7**$^+$ has been confirmed chemically and spectroscopically—see below.)

By contrast, the first oxidation wave of the linkage isomer of *trans*-**7**$^+$, *i.e.* *trans*-[(dppm)$(CO)_2${$(EtO)_3P$}Mn(μ-CN)Mn-$(CNBu^t)(NO)(\eta^5$-$C_5H_4Me)]^+$ *trans*-**17**$^+$, occurs at 0.72 V, which compares well with the oxidation potential of mononuclear *trans*-[Mn(CN){$P(OEt)_3$}$(CO)_2$(dppm)] ($E^{o\prime}$ = 0.50 V),[1] indicating oxidation at $Mn_{oct}$. The potential for the second process for *trans*-**17**$^+$ (1.21 V) compares with that of $[Mn(CNBu^t)(NCMe)(NO)(\eta^5$-$C_5H_4Me)]^+$ ($E^{o\prime}$ = 1.23 V).[3]

Thus, although in each case $Mn_{oct}$ is oxidised first, reversal of the cyanide bridge leads to a different route for MMCT from Mn(I) to Mn(II) in the resulting dication, *i.e. via* C then N in *trans*-**7**$^{2+}$ but from N to C in *trans*-**17**$^{2+}$.

A comparison of *trans*-[(dppm)$(CO)_2${$(EtO)_3P$}Mn(μ-CN)MnL′$(NO)(\eta^5$-$C_5H_4Me)]^+$ {L = $PPh_3$ *trans*-**15**$^+$, $P(OPh)_3$ *trans*-**16**$^+$, $CNBu^t$ *trans*-**17**$^+$ or CNXyl *trans*-**18**$^+$} shows that the first oxidation potential (Table 5) is relatively unchanged while the second decreases in the order $P(OPh)_3$ > CNXyl > $CNBu^t$ > $PPh_3$. Thus, the first oxidation occurs at the *C*-bound octahedral centre. Indeed, further comparisons indicate that the first oxidation for all of *trans*-**1**$^+$–**20**$^+$ occurs at $Mn_{oct}$, *i.e.* the order of oxidation of the two metal centres is independent of L, L′ and R as well as the μ-CN orientation (in marked contrast to the *cis* isomers described above).

This therefore shows that the *cis* or *trans* arrangement of the $Mn(CO)_2$ fragment can also alter the oxidation order, as shown above for *cis*- and *trans*-[(dppm)$(CO)_2${$(PhO)_3P$}Mn(μ-NC)Mn$(CNBu^t)(NO)(\eta^5$-$C_5Me_5)]^+$, *cis*-**9**$^+$ and *trans*-**9**$^+$, and *cis*- and *trans*-[(dppm)$(CO)_2${$(PhO)_3P$}Mn(μ-CN)Mn{$P(OPh)_3$}-$(NO)(\eta^5$-$C_5H_4Me)]^+$, *cis*-**12**$^+$ and *trans*-**12**$^+$. To underline this point, the order of oxidation of the metal centres for both **9**$^+$ and **12**$^+$ is described by Scheme 4. The first oxidation in the *cis* complexes occurs at $Mn_{tet}$ and the second at $Mn_{oct}$. However, after isomerisation the first site to be reduced is $Mn_{tet}$, *i.e.* the order

 

**Table 6** Analytical data for *trans*-[(dppm)(CO)$_2$LMn(μ-NC)MnL′(NO)(η$^5$-C$_5$R$_4$Me)][PF$_6$]$_2$

| | | | | | Analysis (%)[b] | | | IR[c]/cm$^{-1}$ | | | |
|---|---|---|---|---|---|---|---|---|---|---|---|
| Complex[a] | L | L′ | R | Yield (%) | C | H | N | *ν*(CNR) | *ν*(CN) | *ν*(CO) | *ν*(NO) |
| *trans*-**1**$^{2+}$ | P(OPh)$_3$ | PPh$_3$ | H | 67 | 50.1 (50.3) | 3.8 (3.7) | 1.7 (1.8) | — | 2052ms | 2068 w.sh, 1999 | 1752 |
| *trans*-**2**$^{2+}$ | P(OPh)$_3$ | P(OPh)$_3$ | H | 56 | 51.7 (51.8)[d] | 3.7 (3.7) | 1.7 (1.7) | — | 2077m | 2067m, 2002 | 1772 |
| *trans*-**3**$^{2+}$ | P(OPh)$_3$ | CNBu$^t$ | H | 75 | 48.8 (50.0) | 3.5 (3.9) | 3.3 (3.1) | 2177 | 2081 m | 2069 m, 2005 | 1774 |
| *trans*-**4**$^{2+}$ | P(OPh)$_3$ | CNXyl | H | 70 | 51.2 (51.7) | 4.0 (3.8) | 2.5 (3.0) | 2154 | 2085m | 2072m.sh, 2006 | 1777 |
| *trans*-**5**$^{2+}$ | P(OEt)$_3$ | PPh$_3$ | H | 35 | 49.9 (49.6) | 3.9 (4.2) | 2.2 (2.0) | — | 2054ms | 2065 m.sh, 1992 | 1752 |
| *trans*-**6**$^{2+}$ | P(OEt)$_3$ | P(OPh)$_3$ | H | 77 | 47.7 (48.0) | 4.2 (4.1) | 1.8 (1.9) | — | 2079m | 2065sh, 1995 | 1773 |
| *trans*-**7**$^{2+}$ | P(OEt)$_3$ | CNBu$^t$ | H | 79 | 44.5 (44.1) | 4.4 (4.4) | 2.9 (3.4) | 2176 | 2084m | 2069sh, 1997 | 1774 |
| *trans*-**8**$^{2+}$ | P(OEt)$_3$ | CNXyl | H | 62 | 44.2 (44.4) | 4.3 (4.1) | 2.7 (3.1) | 2153 | 2088m | 2071w.sh, 1996 | 1776 |
| *trans*-**9**$^{2+}$ | P(OPh)$_3$ | CNBu$^t$ | Me | 54 | 45.7 (46.0)[e] | 4.5 (4.8) | 3.2 (3.3) | 2162 | 2058 | 2000 | 1755 |
| *trans*-**10**$^{2+}$ | P(OEt)$_3$ | CNBu$^t$ | Me | 48 | 51.4 (51.4) | 4.5 (4.3) | 2.9 (3.0) | 2163 | 2060m | 2072m, 1994 | 1755 |

[a] Isolated as [PF$_6$]$^-$ salts. [b] Calculated values in parentheses. [c] Strong absorptions in $CH_2Cl_2$, unless otherwise stated; w = weak, m = medium, sh = shoulder. [d] Analysed as a 2 : 1 $CH_2Cl_2$ solvate. [e] Analysed as a 1 : 1 $CH_2Cl_2$ solvate.

of oxidation of the monocation is not the reverse of the order of reduction of the trication.

Finally, the different redox behaviour for linkage isomers reflects the σ-donor and π-acceptor properties of the cyanide ligand. Thus, for a pair of linkage isomers in *trans*-**1**$^+$–**20**$^+$, that with the more electron-rich fragment bound to the N atom is approximately 0.2 V easier to oxidise than that bound to C (*cf.* $E_1^{\circ\prime} = 0.55$ V for *trans*-**7**$^+$ and 0.72 V for *trans*-**17**$^+$). When the second process is detectable by cyclic voltammetry, the difference in oxidation potentials, $\Delta E^{\circ\prime}$ ($\Delta E^{\circ\prime} = E_2^{\circ\prime} - E_1^{\circ\prime}$) also varies for linkage isomers, being 0.81 and 0.49 V for *trans*-**7**$^+$ and *trans*-**17**$^+$ respectively as a representative example. The consequences for the electronic spectra of the mixed valence dications *trans*-[(dppm)(CO)$_2$LMn(μ-XY)MnL′(NO)(η$^5$-C$_5$R$_4$Me)]$^{2+}$ are noted below.

### The synthesis and characterisation of the mixed valence dications 1$^{2+}$–20$^{2+}$

With the exceptions of *cis*-[(dppm)(CO)$_2${(PhO)$_3$P}Mn(μ-NC)Mn(PPh$_3$)(NO)(η$^5$-C$_5$H$_4$Me)]$^+$ *cis*-**1**$^+$ and *cis*-[(dppm)(CO)$_2$-{(PhO)$_3$P}Mn(μ-NC)Mn(CNBu$^t$)(NO)(η$^5$-C$_5$Me$_5$)]$^+$ *cis*-**9**$^+$, all of the *cis* and *trans* isomers of [(dppm)(CO)$_2$LMn(μ-NC)MnL′(NO)(η$^5$-C$_5$R$_4$Me)]$^+$ **1**$^+$–**10**$^+$ react with the one-electron oxidant [NO][PF$_6$] to form the corresponding dications *trans*-**1**$^{2+}$–**10**$^{2+}$. (The oxidation of *cis*-**1**$^+$ and *cis*-**9**$^+$, at *C*-bound Mn$_{tet}$, gave dications which are not stable at room temperature although spectroelectrochemistry at −30 °C provides evidence for *cis*-**9**$^{2+}$ at lower temperatures—see below.) By contrast, chemical one-electron oxidation of the linkage isomers [(dppm)(CO)$_2$LMn(μ-CN)MnL′(NO)(η$^5$-C$_5$R$_4$Me)]$^+$ **11**$^+$–**20**$^+$ with [Fe(η$^5$-C$_5$H$_5$)(η$^5$-C$_5$H$_4$COMe)][PF$_6$], [NO][PF$_6$] or [N(C$_6$H$_4$Br-*p*)$_3$][SbCl$_6$] led to decomposition even at low temperature (although, again, low temperature spectroelectrochemistry suggests some stability for *trans*-**17**$^{2+}$).

The most convenient route to the purple mixed-valence salts *trans*-**1**$^{2+}$–**10**$^{2+}$2[PF$_6$]$^-$ involves treatment of *trans*-[(dppm)(CO)$_2$LMn(μ-NC)MnL′(NO)(η$^5$-C$_5$R$_4$Me)]$^+$ *trans*-**1**$^+$–**10**$^+$ in $CH_2Cl_2$ with one equivalent of [NO][PF$_6$]. The solid products decompose significantly within 4 weeks, even when stored under argon at −20 °C, to a mixture containing the *cis* and *trans* monocations; they are soluble in polar solvents such as $CH_2Cl_2$, $CHCl_3$, thf, acetone and dmf, giving very air-sensitive solutions. Nevertheless, *trans*-**1**$^{2+}$–**10**$^{2+}$2[PF$_6$]$^-$ were characterised by elemental analysis (Table 6), cyclic voltammetry (each dication shows one oxidation and one reduction wave at potentials identical to those of the two oxidation waves of the corresponding monocation *trans*-**1**$^+$–**10**$^+$) and IR spectroscopy (Table 6).

Each dication, *trans*-**1**$^{2+}$–**10**$^{2+}$, shows two IR carbonyl bands of different intensity. The stronger absorption is shifted to higher wavenumber with respect to that of the corresponding monocation by *ca.* 80 cm$^{-1}$; the second absorption, assigned to the symmetric stretch of the *trans*-Mn(CO)$_2$ fragment, is also shifted (by *ca.* 60 cm$^{-1}$) but, more significantly, it is more intense when compared to that of the monocations. Similar behaviour has been found on one-electron oxidation of species such as [(H$_3$N)$_5$Ru$^{II}$(μ-NC)Mn$^I$(CO)$_2${P(OPh)$_3$}(dppm)-*trans*]$^{2+}$, with the increased intensity of the symmetric stretch resulting from coupling with the cyanide stretching vibration.[13]

The absorptions corresponding to the nitrosyl and, when present, isocyanide ligands are also shifted to higher wavenumber with respect to the monocations, but by only *ca.* 10 cm$^{-1}$. Thus, the larger energy shift in the carbonyl bands confirms that oxidation of the *trans* monocations occurs at Mn$_{oct}$ which also leads to a lower energy bridging cyanide band (decreased by *ca.* 40 cm$^{-1}$ with respect to that of the monocations).

Addition of one equivalent of [NO][PF$_6$] to a solution of the dication *trans*-[(dppm)(CO)$_2${(EtO)$_3$P}Mn(μ-NC)Mn(CNBu$^t$)(NO)(η$^5$-C$_5$Me$_5$)]$^{2+}$ *trans*-**10**$^{2+}$ led to the formation of a complex showing *ν*(CNR) and *ν*(NO) shifted by *ca.* 70 cm$^{-1}$ to higher wavenumbers and *ν*(CO) shifted to higher energy by 10 cm$^{-1}$, suggesting oxidation at *C*-bound Mn$_{tet}$ and some stability for *trans*-**10**$^{3+}$. However, this trication could not be isolated.

Although only *trans*-**1**$^{2+}$–**10**$^{2+}$ proved isolable, other less stable dications (and one trication) were characterised in solution by low temperature IR spectroelectrochemistry, *i.e.* on *trans*-[(dppm)(CO)$_2${(EtO)$_3$P}Mn(μ-XY)Mn(CNBu$^t$)(NO)(η$^5$-C$_5$H$_4$Me)]$^+$ (XY = NC, *trans*-**7**$^+$; XY = CN, *trans*-**17**$^+$) and *cis*-[(dppm)(CO)$_2${(PhO)$_3$P}Mn(μ-NC)Mn(CNBu$^t$)(NO)(η$^5$-C$_5$Me$_5$)]$^+$ *cis*-**9**$^+$.

Electrolysis of *trans*-**7**$^+$ at an applied potential, $E_{app}$, of 0.6 V (*vs.* a Ag wire electrode) at −30 °C in $CH_2Cl_2$, resulted in the *ν*(CO) band at 1914 cm$^{-1}$ collapsing and a new band forming at 1998 cm$^{-1}$. Increases of *ca.* 13 cm$^{-1}$ and 8 cm$^{-1}$ were observed

for $\nu$(NO) and $\nu$(CNR) respectively; the $\nu$(CN) band decreased in energy by 48 $cm^{-1}$ and became more intense. Thus, the shifts in all of the bands are consistent with oxidation at the *N*-bound *trans*-$Mn(CO)_2$ centre, generating *trans*-[(dppm)$(CO)_2${$(EtO)_3P$}Mn(μ-NC)Mn($CNBu^t$)(NO)($\eta^5$-$C_5H_4Me$)]$^{2+}$ *trans*-**7**$^{2+}$ (*cf.* the isolated salt *trans*-**7**$^{2+}$2[$PF_6$]$^-$, see above).

Increasing $E_{app}$ to 1.45 V resulted in increases in energy for $\nu$(CO), $\nu$(NO) and $\nu$(CNR) of 16, 101 and 62 $cm^{-1}$ respectively, this time consistent with oxidation at the *C*-bound manganese centre and the generation of *trans*-**7**$^{3+}$. Lowering $E_{app}$ to 0.6 V and then to 0.0 V regenerated *trans*-**7**$^{2+}$ and *trans*-**7**$^{+}$ respectively, with the intensities of the corresponding IR bands greater than 85% of those observed in the forward process. Thus, the trication *trans*-**7**$^{3+}$ and the dication *trans*-**7**$^{2+}$ appear to be stable in $CH_2Cl_2$ at −30 °C.

Electrolysis at 0.72 V of *trans*-**17**$^{+}$, the linkage isomer of *trans*-**7**$^{+}$, at −30 °C in $CH_2Cl_2$, resulted in a large increase in the energy of the carbonyl bands, while $\nu$(NO) and $\nu$(CNR) move to higher energy by only 8 and 12 $cm^{-1}$. Thus, oxidation at $Mn_{oct}$, as proposed on the basis of cyclic voltammetry, gave *trans*-[(dppm)$(CO)_2${$(EtO)_3P$}Mn(μ-CN)Mn($CNBu^t$)(NO)($\eta^5$-$C_5H_4Me$)]$^{2+}$ *trans*-**17**$^{2+}$. Lowering $E_{app}$ to 0.0 V regenerated *trans*-**17**$^{+}$, confirming that the dication *trans*-**17**$^{2+}$ is stable at −30 °C (although not isolable at room temperature). By contrast, increasing $E_{app}$ to 1.21 V to generate *trans*-**17**$^{3+}$ resulted in sample decomposition.

Cyclic voltammetry of *cis*-[(dppm)$(CO)_2${$(PhO)_3P$}Mn(μ-NC)Mn($PPh_3$)(NO)($\eta^5$-$C_5H_4Me$)]$^{+}$ *cis*-**1**$^{+}$ and *cis*-[(dppm)$(CO)_2${$(PhO)_3P$}Mn(μ-NC)Mn($CNBu^t$)(NO)($\eta^5$-$C_5Me_5$)]$^{+}$ *cis*-**9**$^{+}$ indicated reversible one-electron oxidation at $Mn_{tet}$ but chemical oxidation at room temperature led to sample decomposition. However, at −30 °C IR spectroelectrochemistry of *cis*-**9**$^{+}$, at $E_{app}$ = 1.0 V, led to an increase in energy for $\nu$(NO) and $\nu$(CNR) of 94 and 69 $cm^{-1}$, but only a small increase for one of the $\nu$(CO) bands. Thus, the formation of *cis*-**9**$^{2+}$ again confirmed the assignment made on the basis of cyclic voltammetry. Lowering $E_{app}$ to 0.0 V regenerated *cis*-**9**$^{+}$, with the intensities of the bands greater than 90% of those observed in the forward process, indicating stability of the dication *cis*-**9**$^{2+}$ in $CH_2Cl_2$ at −30 °C.

### The electronic spectra of the mixed valence dications *trans*-**1**$^{2+}$–**10**$^{2+}$

The electronic spectra of *trans*-**1**$^{+}$–**10**$^{+}$ and the mononuclear cyanomanganese(I) precursors [Mn(CN)L′(NO)($\eta^5$-$C_5R_4Me$)] and *trans*-[MnBrL$(CO)_2$(dppm)] show no absorptions above 400 nm. However, the dications *trans*-**1**$^{2+}$–**10**$^{2+}$ show two distinct absorptions in $CH_2Cl_2$, one in the visible or near-IR region and a second weaker band at higher energy (Table 7), *e.g.* *trans*-**3**$^{2+}$ shows absorptions at 504 nm ($\varepsilon$ = 1061 $dm^3$ $mol^{-1}$ $cm^{-1}$) and 972 nm ($\varepsilon$ = 2633 $dm^3$ $mol^{-1}$ $cm^{-1}$). The lower energy bands are assigned to optically induced metal–metal charge-transfer (MMCT) from Mn(I) to Mn(II) centre *via* the cyanide bridge as they are solvatochromic (see below); the higher energy bands are essentially unaffected by the solvent.

A comparison of the electronic spectral data for *trans*-**1**$^{2+}$–**10**$^{2+}$ shows that the energy of the MMCT band varies with the ligands at the two manganese centres. Fig. 10 shows the spectra of *trans*-[(dppm)$(CO)_2${$(EtO)_3P$}Mn(μ-NC)Mn($CNBu^t$)(NO)($\eta^5$-$C_5R_4Me$)]$^{2+}$ (R = H, *trans*-**7**$^{2+}$; R = Me, *trans*-**10**$^{2+}$). The higher

**Table 7** Electronic spectroscopic data for *trans*-[(dppm)$(CO)_2$LMn(μ-NC)MnL′(NO)($\eta^5$-$C_5R_4Me$)]$^{2+}$ in $CH_2Cl_2$

| Complex | L | L′ | R | $\lambda_{max}$/nm ($\varepsilon$/$dm^3$ $mol^{-1}$ $cm^{-1}$) |
|---|---|---|---|---|
| *trans*-**1**$^{2+}$ | $P(OPh)_3$ | $PPh_3$ | H | 501 (990), 1100 (3350) |
| *trans*-**2**$^{2+}$ | $P(OPh)_3$ | $P(OPh)_3$ | H | 503 (—[a]), 852 (2930) |
| *trans*-**3**$^{2+}$ | $P(OPh)_3$ | $CNBu^t$ | H | 504 (1061), 972 (2633) |
| *trans*-**4**$^{2+}$ | $P(OPh)_3$ | CNXyl | H | 504 (1078), 948 (2096) |
| *trans*-**5**$^{2+}$ | $P(OEt)_3$ | $PPh_3$ | H | 500 (1135), 1004 (2523) |
| *trans*-**6**$^{2+}$ | $P(OEt)_3$ | $P(OPh)_3$ | H | 464 (—[a]), 811 (2909) |
| *trans*-**7**$^{2+}$ | $P(OEt)_3$ | $CNBu^t$ | H | 488 (1490), 877 (2685) |
| *trans*-**8**$^{2+}$ | $P(OEt)_3$ | CNXyl | H | 500 (1148), 856 (1409) |
| *trans*-**9**$^{2+}$ | $P(OPh)_3$ | $CNBu^t$ | Me | 504 (1236), 1180 (2955) |
| *trans*-**10**$^{2+}$ | $P(OEt)_3$ | $CNBu^t$ | Me | 499 (1310), 1021 (3460) |

[a] Not determined due to ill-defined bands.

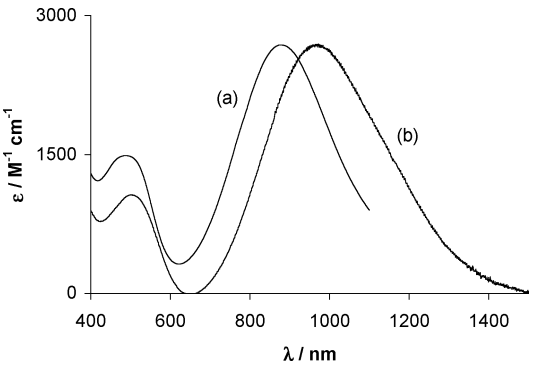


**Fig. 10** The electronic spectra of (a) *trans*-[(dppm)$(CO)_2${$(EtO)_3P$}Mn(μ-NC)Mn($CNBu^t$)(NO)($\eta^5$-$C_5H_4Me$)]$^{2+}$ *trans*-**7**$^{2+}$ and (b) *trans*-[(dppm)$(CO)_2${$(EtO)_3P$}Mn(μ-NC)Mn($CNBu^t$)(NO)($\eta^5$-$C_5Me_5$)]$^{2+}$ *trans*-**10**$^{2+}$ in $CH_2Cl_2$.

value of $\lambda_{max}$ (1021 nm) for *trans*-**10**$^{2+}$ indicates relatively facile Mn(I) to Mn(II) MMCT compared with *trans*-**7**$^{2+}$ (877 nm).

The electronic spectra of the air-sensitive dications *trans*-**7**$^{2+}$ and *trans*-**17**$^{2+}$ were further studied by *in situ* spectroelectrochemical oxidation of the corresponding monocations *trans*-**7**$^{+}$ and *trans*-**17**$^{+}$ in $CH_2Cl_2$ at −30 °C. In addition, this technique was used to monitor the second oxidation step, to the trications *trans*-[(dppm)$(CO)_2${$(EtO)_3P$}$Mn^{II}$(μ-XY)$Mn^{II}$($CNBu^t$)(NO)($\eta^5$-$C_5H_4Me$)]$^{3+}$ (XY = NC, *trans*-**7**$^{3+}$; XY = CN, *trans*-**17**$^{3+}$). As $E_{app}$ is increased from 0.0 to 0.6 V (*vs.* a Ag/AgCl electrode) the dication *trans*-**7**$^{2+}$ is generated from *trans*-**7**$^{+}$. The octahedral Mn(I) site is oxidised to Mn(II) and the weak absorption at 370 nm loses intensity. More obviously, a MMCT band appears at *ca.* 890 nm, as observed for the isolated dication *trans*-**7**$^{2+}$. A second, less intense band appears at 493 nm. Isosbestic points at 317 and 412 nm suggest that *trans*-**7**$^{+}$ and *trans*-**7**$^{2+}$ are the only absorbing species in solution.

Increasing $E_{app}$ past the $E^{\circ\prime}$ value for the second oxidation step (1.36 V) causes the MMCT band to collapse as the intermetallic interaction is switched off. Lowering $E_{app}$ to 0.6 V regenerates *trans*-**7**$^{2+}$ with the intensity of the corresponding MMCT band greater than 90% of that observed in the forward process. As shown by IR spectroelectrochemistry, *trans*-**7**$^{3+}$ and *trans*-**7**$^{2+}$ appear to be stable in $CH_2Cl_2$ at −30 °C.

The linkage isomer of *trans*-**7**$^{+}$, *i.e.* *trans*-**17**$^{+}$, shows no significant absorptions above 220 nm. However, as $E_{app}$ is increased

 

from 0.0 to 0.7 V, and the dication *trans*-**17**$^{2+}$ is generated, $Mn_{oct}$ is oxidised and a broad MMCT band appears at 1354 nm (with a shoulder towards lower wavelength). A second band, significantly weaker, is observed at 537 nm; two isosbestic points are observed at 305 and 408 nm. The lower energy of the MMCT band for *trans*-**17**$^{2+}$, *cf.* that of *trans*-**7**$^{2+}$, indicates that electron transfer from Mn(I) to Mn(II) in $Mn^{II}_{oct}$–CN–$Mn^{I}_{tet}$ (in *trans*-**17**$^{2+}$) is easier than from Mn(I) to Mn(II) in $Mn^{II}_{oct}$–NC–$Mn^{I}_{tet}$ (of *trans*-**7**$^{2+}$).

Although the effect of the bridging ligand on the extent of intermetallic interaction in mixed-valence complexes has been frequently studied, no such study has been made with respect to cyanide–isocyanide isomerism in dinuclear complexes. Indirect effects of the cyanide orientation have been recorded during the spontaneous isomerisation of [(pc)Fe{(μ-CN)Fe(dppe)(η$^5$-$C_5H_5$)}$_2$]$^+$ (pc = phthalocyaninate) to [(pc)Fe{(μ-NC)Fe(dppe)(η$^5$-$C_5H_5$)}$_2$]$^+$,[14] in which the near-IR spectrum shows a change in the wavelength of the MMCT band from 1293 to 2150 nm. Therefore, the effect of cyanide orientation on the energy of the MMCT band has been studied in *trans*-[(dppm)(CO)$_2${(EtO)$_3$P}$Mn^{II}$(μ-XY)$Mn^{I}$(CNBu$^t$)(NO)(η$^5$-$C_5H_4$Me)]$^{2+}$ (XY = NC, *trans*-**7**$^{2+}$; XY = CN, *trans*-**17**$^{2+}$) as a representative example.

As shown by CV and IR spectroelectrochemistry, the first oxidation of *trans*-**7**$^+$ and *trans*-**17**$^+$ occurs at $Mn_{oct}$. Therefore, MMCT in the mixed-valence species *trans*-[(dppm)(CO)$_2${(EtO)$_3$P}$Mn^{II}$(μ-XY)$Mn^{I}$(CNBu$^t$)(NO)(η$^5$-$C_5H_4$Me)]$^{2+}$ will take place in the same direction, from $Mn_{tet}$ to $Mn_{oct}$, but across a bridging cyanide in two different orientations, *i.e.* from Mn(I) to CN to Mn(II) in *trans*-**7**$^{2+}$ and from Mn(I) to NC to Mn(II) in *trans*-**17**$^{2+}$ (Scheme 5).

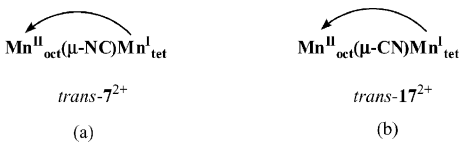


**Scheme 5** The direction of MMCT in the mixed-valence complexes (a) *trans*-[(dppm)(CO)$_2${(EtO)$_3$P}Mn(μ-NC)Mn(CNBu$^t$)(NO)(η$^5$-$C_5H_4$Me)]$^{2+}$ *trans*-**7**$^{2+}$ and (b) *trans*-[(dppm)(CO)$_2${(EtO)$_3$P}Mn(μ-CN)Mn(CNBu$^t$)(NO)(η$^5$-$C_5H_4$Me)]$^{2+}$ *trans*-**17**$^{2+}$.

Hush theory[15] relates the energy of the MMCT band, $E_{op}$, to the ground state free energy difference, $\Delta G^\circ$, and the reorganisation energy, $\chi$, according to eqn (1). In addition, $\Delta G^\circ = -nF\Delta E^{\circ\prime}$, where $\Delta E^{\circ\prime}$ is the difference between the potentials for the two redox processes.

$$E_{op} = \Delta G^\circ + \chi = -nF\Delta E^{\circ\prime} \quad (1)$$

A plot of the energy of the MMCT band, $E_{op}$ in cm$^{-1}$, against $\Delta E^{\circ\prime}$ for *trans*-**1**$^{2+}$–**10**$^{2+}$ and *trans*-**17**$^{2+}$ (obtained by electronic spectroelectrochemistry) (Fig. 11) is approximately linear ($R^2$ = 0.86); as $\Delta E^{\circ\prime}$ decreases, the Mn(I) to Mn(II) electron transfer becomes generally more favourable and thus the MMCT band energy decreases. Such a relationship has also been found for the trinuclear complexes [(pc)Fe{(μ-XY)Ru(PPh$_3$)$_2$(η$^5$-$C_5H_5$)}$_2$] and [(pc)Fe{(μ-XY)Fe(dppe)(η$^5$-$C_5H_5$)}$_2$] (XY = CN or NC).[14]

Although the MMCT band for *trans*-[(dppm)(CO)$_2$LMn(μ-NC)MnL′(NO)(η$^5$-$C_5R_4$Me)]$^{2+}$ *trans*-**1**$^{2+}$–**10**$^{2+}$ is solvatochromic, it is rather weakly so. (Data for *trans*-**2**$^{2+}$ in four solvents are given in Table 8; those for *trans*-**4**$^{2+}$, *trans*-**6**$^{2+}$–**8**$^{2+}$ and *trans*-**10**$^{2+}$ are given as ESI‡.) This behaviour contrasts markedly with the pronounced solvatochromism exhibited by [X$_3$Fe$^{III}$-(μ-NC)Mn$^{I}$(CO)$_2$L(dppm)-*trans*)][16] and [(H$_3$N)$_5$Ru$^{III}$(μ-NC)Mn$^{I}$-(CO)$_2$L(dppm)-*trans*)]$^{3+}$.[13] For example, *trans*-[(dppm)-(CO)$_2${(PhO)$_3$P}$Mn^{II}$(μ-NC)$Mn^{I}${P(OPh)$_3$}(NO)(η$^5$-$C_5H_4$Me)]$^{2+}$ *trans*-**2**$^{2+}$ shows MMCT bands at 848, 852 and 870 nm in MeCN, $CH_2Cl_2$ and thf respectively, an overall shift of only *ca.* 20 nm. By contrast, the MMCT band of *trans*-[(H$_3$N)$_5$Ru$^{III}$(μ-NC)Mn$^{I}$(CO)$_2${P(OPh)$_3$}(dppm)-*trans*)]$^{3+}$ occurs at 963, 1134 and 946 nm in the same solvents, the overall difference of *ca.* 190 nm resulting from variable hydrogen bonding of the solvent with the Ru$^{III}$(NH$_3$)$_5$ group. Such hydrogen bonding is likely to be much less significant for *trans*-[(dppm)(CO)$_2$LMn(μ-NC)MnL′(NO)(η$^5$-$C_5R_4$Me)]$^{2+}$.

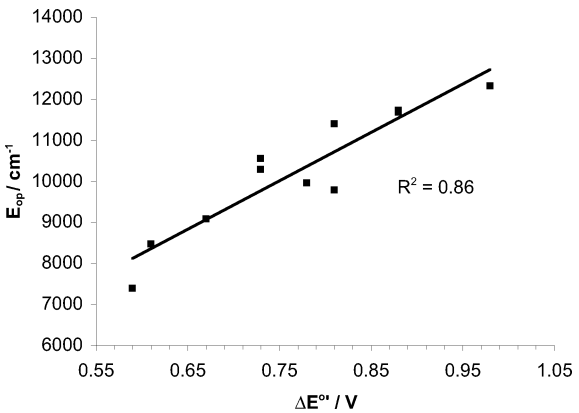


**Fig. 11** Plot of $\Delta E^{\circ\prime}$ *vs.* $E_{op}$ for *trans*-**1**$^{2+}$–**10**$^{2+}$ and *trans*-**17**$^{2+}$.

For mixed-valence species the magnitude of the intermetallic interaction can be expressed in terms of the coupling parameter $J$, in units of cm$^{-1}$, or the degree of electron delocalisation, $\alpha^2$ [eqn (2) and (3)].

$$J = 2.05 \times 10^{-2}[\varepsilon \times \nu_{1/2} \times E]^{1/2} \times r^{-1}\ (\text{cm}^{-1}) \quad (2)$$

$$\alpha^2 = 4.24 \times 10^{-4}[(\varepsilon \times \nu_{1/2})/(E \times r^2)]\ (\%) \quad (3)$$

**Table 8** Metal–metal charge-transfer data for *trans*-[(dppm)(CO)$_2${(PhO)$_3$P}Mn(μ-NC)Mn{P(OPh)$_3$}(NO)(η$^5$-$C_5H_4$Me)]$^{2+}$ *trans*-**2**$^{2+}$

| Solvent | DN [a] | $\lambda_{max}$/nm | $E$/cm$^{-1}$ | $\varepsilon$/dm$^3$ mol$^{-1}$ cm$^{-1}$ | $\nu_{1/2}$/cm$^{-1}$ | $J$/cm$^{-1}$ | $\alpha^2$ (%) |
|---|---|---|---|---|---|---|---|
| $CH_2Cl_2$ | 1.0 | 852 | 11737 | 2930 | 3530 | 1403 | 1.43 |
| MeCN | 14.1 | 848 | 11792 | 2550 | 3501 | 1302 | 1.22 |
| acetone | 17.0 | 855 | 11692 | 2834 | 3650 | 1395 | 1.42 |
| thf | 20.0 | 870 | 11494 | 2725 | 3642 | 1355 | 1.39 |

[a] DN = Gutmann donor number.

Here, $\varepsilon$ is the extinction coefficient for the MMCT band in $dm^3\ mol^{-1}\ cm^{-1}$, $v_{1/2}$ is the width of the band at half-height in $cm^{-1}$, $E$ is the energy of the band maximum in $cm^{-1}$ and $r$ is the metal–metal separation in Å.

Values of $J$ and $\alpha^2$ for *trans*-$\mathbf{2}^{2+}$ are given in Table 8, and for *trans*-$\mathbf{4}^{2+}$, *trans*-$\mathbf{6}^{2+}$-$\mathbf{8}^{2+}$ and *trans*-$\mathbf{10}^{2+}$ in the ESI.‡ (The value of $r$ = 5.110 Å, the metal–metal separation along the Mn–C–N–Mn linkage, was calculated from the X-ray structure of *trans*-[(dppm)$(CO)_2${$(EtO)_3P$}Mn(μ-NC)Mn$(CNBu^t)(NO)(\eta^5$-$C_5H_4Me)]^+$ *trans*-$\mathbf{7}^+$. The through space distance is insignificantly different, at 5.096 Å.)

The values of $J$ for *trans*-$\mathbf{1}^{2+}$–$\mathbf{10}^{2+}$ in $CH_2Cl_2$ vary only modestly, ranging from 1513 $cm^{-1}$ for *trans*-$\mathbf{6}^{2+}$ to 967 $cm^{-1}$ for *trans*-$\mathbf{8}^{2+}$, and are generally smaller than those of other mixed-valence complexes containing cyanomanganese ligands, such as $[(H_3N)_5Ru(\mu$-NC)MnL′$(NO)(\eta^5$-$C_5H_4Me)]^{3+}$ {L′ = $PPh_3$ or $P(OPh)_3$}[13] or $[X_3Fe(\mu$-NC)$MnL_x]$ {$L_x$ = *cis*- or *trans*-$(CO)_2${$P(OR)_3$}(dppm); R = OPh or OEt}.[16] The computed values of $\alpha^2$, the degree of delocalisation, are consistent with the assignment of *trans*-$\mathbf{1}^{2+}$–$\mathbf{10}^{2+}$ as Class II mixed-valence complexes.

## Conclusions

The reaction of cyanomanganese complexes [Mn(CN)L′$(NO)(\eta^5$-$C_5R_4Me)]$ with *cis*- or *trans*-[MnBrL$(CO)_2$(dppm)] in the presence of Tl[$PF_6$] gives homobinuclear cyanomanganese(I) species of the general formula *cis*- or *trans*-[(dppm)$(CO)_2$LMn(μ-NC)MnL′$(NO)(\eta^5$-$C_5R_4Me)]^+$ $\mathbf{1}^+$–$\mathbf{10}^+$. The linkage isomers of $\mathbf{1}^+$–$\mathbf{10}^+$, namely *cis*- or *trans*-[(dppm)$(CO)_2$LMn(μ-CN)-MnL′$(NO)(\eta^5$-$C_5R_4Me)]^+$ $\mathbf{11}^+$–$\mathbf{20}^+$, were synthesised by reacting the cyanomanganese ligands *cis*- or *trans*-[Mn(CN)L-$(CO)_2$(dppm)] with [MnIL′$(NO)(\eta^5$-$C_5R_4Me)]$ in the presence of Tl[$PF_6$].

The linkage isomers *trans*-[(dppm)$(CO)_2${$(EtO)_3P$}Mn(μ-NC)Mn$(CNBu^t)(NO)(\eta^5$-$C_5H_4Me)]^+$ *trans*-$\mathbf{7}^+$ and *trans*-[(dppm)-$(CO)_2${$(EtO)_3P$}Mn(μ-CN)Mn$(CNBu^t)(NO)(\eta^5$-$C_5H_4Me)]^+$ *trans*-$\mathbf{17}^+$ are isostructural but *cis*-[(dppm)$(CO)_2${$(PhO)_3P$}Mn(μ-NC)Mn{$P(OPh)_3$}$(NO)(\eta^5$-$C_5H_4Me)]^+$ *cis*-$\mathbf{2}^+$ and *cis*-[(dppm)-$(CO)_2${$(PhO)_3P$}Mn(μ-CN)Mn{$P(OPh)_3$}$(NO)(\eta^5$-$C_5H_4Me)]^+$ *cis*-$\mathbf{12}^+$ differ by coordination of two different optical isomers of the *pseudo*-tetrahedral unit.

The cations *cis*- and *trans*-$\mathbf{1}^+$–$\mathbf{20}^+$ undergo sequential oxidation of the two Mn(I) centres to Mn(II); the redox-induced isomerisation observed for units containing the *cis*-$Mn(CO)_2$ fragment allows assignment of the order of oxidation of the *cis* isomers. This order may be controlled by systematic variation of the ligands L and L′, the substituents on the cyclopentadienyl ring and the μ-CN orientation.

One-electron oxidation of *trans*-[(dppm)$(CO)_2$LMn$^I$(μ-NC)Mn$^I$L′$(NO)(\eta^5$-$C_5R_4Me)]^+$ *trans*-$\mathbf{1}^+$–$\mathbf{10}^+$ with [NO][$PF_6$] in $CH_2Cl_2$ forms the dications *trans*-$\mathbf{1}^{2+}$–$\mathbf{10}^{2+}$ which are also obtained by oxidising *cis*-[(dppm)$(CO)_2$LMn$^I$(μ-NC)Mn$^I$L′$(NO)(\eta^5$-$C_5R_4Me)]^+$ *cis*-$\mathbf{1}^+$–$\mathbf{10}^+$ by *cis*–*trans* isomerisation at the octahedral $Mn(CO)_2$ site.

The dications show weakly solvatochromic MMCT bands consistent with Class II mixed-valency. The energy of these bands is affected by the orientation of the cyanide bridge such that electron transfer from Mn(I) to Mn(II) through the unit $Mn^{II}$(μ-NC)$Mn^I$ in *trans*-[(dppm)$(CO)_2${$(EtO)_3P$}$Mn^{II}$(μ-NC)$Mn^I$-$(CNBu^t)(NO)(\eta^5$-$C_5H_4Me)]^{2+}$ *trans*-$\mathbf{7}^{2+}$ occurs at higher energy than through the $Mn^{II}$(μ-CN)$Mn^I$ in the linkage isomer *trans*-[(dppm)$(CO)_2${$(EtO)_3P$}$Mn^{II}$(μ-CN)$Mn^I(CNBu^t)(NO)(\eta^5$-$C_5H_4Me)]^{2+}$ *trans*-$\mathbf{17}^{2+}$.

## Experimental

The preparation, purification and reactions of the complexes described were carried out under an atmosphere of dry nitrogen using dried and deoxygenated solvents purified either by distillation or by using Anhydrous Engineering double alumina or alumina–copper catalyst drying columns. Reactions were monitored by IR spectroscopy where necessary. Unless stated otherwise, complexes were purified using a mixture of two solvents. The impure solid was dissolved in the more polar solvent, the resulting solution was filtered and then treated with the second solvent, and the mixture was reduced in volume *in vacuo* to induce precipitation. Unless otherwise stated, complexes are stable under nitrogen and dissolve in polar solvents such as $CH_2Cl_2$, thf and acetone to give moderately air-stable solutions.

The compounds *trans*- and *cis*-[Mn(CN)$(CO)_2$L(dppm)] {L = $P(OEt)_3$[1] and $P(OPh)_3$[17]} and [MnBr$(CO)_2$L(dppm)] {L = $P(OEt)_3$[1] and $P(OPh)_3$},[18] [Mn(CO)$(PPh_3)(NO)(\eta^5$-$C_5H_4Me)][PF_6]$,[19] [Mn(CN)$(PR_3)(NO)(\eta^5$-$C_5H_4Me)]$ (R = Ph and OPh),[20,21] $[Fe(\eta^5$-$C_5H_5)_2][PF_6]$,[22] and $[Fe(\eta^5$-$C_5H_5)(\eta^5$-$C_5H_4COMe)][PF_6]$[22] were prepared by published methods. The compounds [NO][$PF_6$], CNXyl and $CNBu^t$ were purchased from Aldrich and Tl[$PF_6$] was purchased from Strem Chemicals.

IR spectra were recorded on a Nicolet 5ZDX FT spectrometer. Electrochemical studies were carried out using an EG&G Model 273A potentiostat linked to a computer using EG&G Model 270 Research Electrochemistry software in conjunction with a three-electrode cell. The auxiliary electrode was a platinum wire and the working electrode a platinum disc (1.6 mm diameter). The reference was an aqueous saturated calomel electrode separated from the test solution by a fine porosity frit and an agar bridge saturated with KCl. Solutions were $5.0 \times 10^{-4}$ or $1.0 \times 10^{-3}$ mol $dm^{-3}$ in the test compound and 0.1 mol $dm^{-3}$ in $[NBu^n_4][PF_6]$ as the supporting electrolyte with $CH_2Cl_2$ as the solvent. Under these conditions, $E^{\circ\prime}$ for the one-electron oxidation of $[Fe(\eta^5$-$C_5Me_5)_2]$, added to the test solutions as an internal calibrant, is −0.08 V. UV-visible spectra were recorded on a Perkin Elmer Lambda 2 spectrometer using 1.0 cm path length quartz cells. UV-visible-near-IR spectra were recorded on a Perkin Elmer Lambda 19 spectrometer using 0.1 cm path length quartz cells. UV-visible-near-IR spectroelectrochemical measurements were made using an EG&G model 273A potentiostat in conjunction with a three-electrode system fitted to the Perkin Elmer Lambda 19 spectrometer. IR spectroelectrochemical measurements were made in conjunction with a three-electrode system fitted to a Bruker IFS25 Spectrometer.

Microanalyses were carried out by the staff of the Microanalysis Service of the School of Chemistry, University of Bristol.

### Syntheses

***cis*-[(dppm)$(CO)_2${$(PhO)_3P$}Mn(μ-NC)Mn$(PPh_3)(NO)(\eta^5$-$C_5H_4$-Me)][$PF_6$] *cis*-$\mathbf{1}^+[PF_6]^-$.** To a stirred solution of [Mn(CN)-$(PPh_3)(NO)(\eta^5$-$C_5H_4Me)]$ (67 mg, 0.15 mmol) and *cis*-[MnBr$(CO)_2${$P(OPh)_3$}(dppm)] (130 mg, 0.15 mmol) in $CH_2Cl_2$

 

(20 $cm^3$) was added $Tl[PF_6]$ (54 mg, 0.15 mmol). After 24 h the orange solution was filtered through Celite and evaporated to dryness *in vacuo*. After washing the product with toluene (2 × 10 $cm^3$), the orange residue was purified using $CH_2Cl_2$–*n*-hexane to give an orange crystalline solid, yield 129 mg (63%).

The complexes *cis*-**2**$^+[PF_6]^-$–*cis*-**8**$^+[PF_6]^-$ were prepared similarly, although the reaction times varied from 24 h to 72 h. Complexes *trans*-**1**$^+[PF_6]^-$–*trans*-**6**$^+[PF_6]^-$, *trans*-**9**$^+[PF_6]^-$ and *trans*-**10**$^+[PF_6]^-$ were prepared similarly by using *trans*-$[MnBr(CO)_2\{P(OR)_3\}(dppm)]$.

***cis*-[(dppm)(CO)$_2${(PhO)$_3$P}Mn(μ-NC)Mn(CNBu$^t$)(NO)(η$^5$-C$_5$Me$_5$)][PF$_6$] *cis*-9$^+$[PF$_6$]$^-$.** To a stirred solution of $[Mn(CN)(CNBu^t)(NO)(\eta^5\text{-}C_5Me_5)]$ (26 mg, 0.08 mmol) and *cis*-$[MnBr(CO)_2\{P(OPh)_3\}(dppm)]$ (70 mg, 0.08 mmol) in $CH_2Cl_2$ (15 $cm^3$) was added $Tl[PF_6]$ (31 mg, 0.09 mmol). After 24 h the orange solution was filtered through Celite and the volume of the solution reduced to *ca.* 5 $cm^3$. After adding *n*-hexane (5 $cm^3$) the volume of the solution was reduced *in vacuo* to leave an orange solid, yield 72 mg (72%).

The complex *cis*-$[(dppm)(CO)_2\{(EtO)_3P\}Mn(\mu\text{-}NC)Mn(CNBu^t)(NO)(\eta^5\text{-}C_5Me_5)][PF_6]$ *cis*-**10**$^+[PF_6]^-$ was prepared similarly as a red solid.

***trans*-[(dppm)(CO)$_2${(EtO)$_3$P}Mn(μ-NC)Mn(CNXyl)(NO)(η$^5$-C$_5$H$_4$Me)][PF$_6$] *trans*-8$^+$[PF$_6$]$^-$.** To a stirred solution of *cis*-$[(dppm)(CO)_2\{(EtO)_3P\}Mn(\mu\text{-}NC)Mn(CNXyl)(NO)(\eta^5\text{-}C_5H_4\text{-}Me)][PF_6]$ *cis*-**8**$^+[PF_6]^-$ (100 mg, 0.09 mmol) in $CH_2Cl_2$ (15 $cm^3$) was added $[NO][PF_6]$ (17 mg, 0.10 mmol). After 15 min, $N_2H_4{\cdot}xH_2O$ (0.3 $cm^3$) was added to the purple solution. The resulting orange solution was stirred for 15 min in the presence of $MgSO_4$ and then filtered through Celite. Addition of *n*-hexane (15 $cm^3$) induced precipitation of a solid which was purified using $CH_2Cl_2$–*n*-hexane to give a crystalline orange solid, yield 54 mg (54%).

The complex *trans*-$[(dppm)(CO)_2\{(EtO)_3P\}Mn(\mu\text{-}NC)Mn(CNBu^t)(NO)(\eta^5\text{-}C_5H_4Me)][PF_6]$ *trans*-**7**$^+[PF_6]^-$ was prepared similarly as a yellow solid.

***cis*-[(dppm)(CO)$_2${(EtO)$_3$P}Mn(μ-CN)Mn(CNBu$^t$)(NO)(η$^5$-C$_5$H$_4$Me)][PF$_6$] *cis*-17$^+$[PF$_6$]$^-$.** To a stirred solution of *cis*-$[Mn(CN)(CO)_2\{P(OEt)_3\}(dppm)]$ (200 mg, 0.29 mmol) and $[MnI(CNBu^t)(NO)(\eta^5\text{-}C_5H_4Me)]$ (109 mg, 0.29 mmol) in $CH_2Cl_2$ (15 $cm^3$) was added $Tl[PF_6]$ (112 mg, 0.32 mmol). After 50 min the red solution was filtered through Celite and the volume of the filtrate reduced to *ca.* 5 $cm^3$. After adding *n*-hexane (5 $cm^3$) the volume of the solution was reduced *in vacuo* to induce precipitation of a pink solid which was thoroughly washed with diethyl ether (3 × 10 $cm^3$), yield 220 mg (70%).

The complexes *cis*- or *trans*-**11**$^+[PF_6]^-$–**18**$^+[PF_6]^-$, except *cis*-**15**$^+[PF_6]^-$, were prepared similarly with the following modifications: *trans*-**17**$^+[PF_6]^-$ and *trans*-**18**$^+[PF_6]^-$ were purified using $CH_2Cl_2$–*n*-hexane; the reaction time for *cis*-**11**$^+[PF_6]^-$ was 2 h.

***cis*-[(dppm)(CO)$_2${(EtO)$_3$P}Mn(μ-CN)Mn(PPh$_3$)(NO)(η$^5$-C$_5$H$_4$Me)][PF$_6$] *cis*-15$^+$[PF$_6$]$^-$.** To a stirred solution of *cis*-$[Mn(CN)(CO)_2\{P(OEt)_3\}(dppm)]$ (150 mg, 0.22 mmol) and $[Mn(CO)(PPh_3)(NO)(\eta^5\text{-}C_5H_4Me)]$ (130 mg, 0.22 mmol) in $CH_2Cl_2$ (25 $cm^3$) was added $Me_3NO$ (16 mg, 0.22 mmol). After 45 min the green solution was filtered through Celite and the

**Table 9** Crystal and refinement data for cyanide-bridged manganese complexes

| Compound | *trans*-**7**$^+[PF_6]^-{\cdot}Me_2CO$ | *trans*-**17**$^+[PF_6]^-{\cdot}Me_2CO$ | *cis*-**12**$^+[PF_6]^-$ | *cis*-**2**$^+[PF_6]^-$ | *cis*-**8**$^+[PF_6]^-\cdot1.5CH_2Cl_2$ | *cis*-**9**$^+[PF_6]^-\cdot CH_2Cl_2$ |
|---|---|---|---|---|---|---|
| Formula | $C_{48}H_{59}F_6Mn_2N_3O_7P_4$ | $C_{48}H_{59}F_6Mn_2N_3O_7P_4$ | $C_{70}H_{59}F_6Mn_2N_2O_9P_5$ | $C_{70}H_{59}F_6Mn_2N_2O_9P_5$ | $C_{50.5}H_{56}Cl_3F_6Mn_2N_3O_6P_4$ | $C_{62}H_{63}Cl_2F_6Mn_2N_3O_6P_4$ |
| *M* | 1137.74 | 1137.74 | 1450.92 | 1450.92 | 1255.09 | 1364.81 |
| Crystal system | Triclinic | Triclinic | Orthorhombic | Monoclinic | Triclinic | Triclinic |
| Space group (no.) | $P\bar{1}$ (2) | $P\bar{1}$ (2) | *Pca*2(1) (29) | *P*2(1)/*c* (14) | $P\bar{1}$ (2) | $P\bar{1}$ (2) |
| *a*/Å | 11.077(4) | 11.0916(15) | 34.821(3) | 18.98(3) | 9.9087(6) | 13.651(2) |
| *b*/Å | 13.608(4) | 13.638(2) | 11.161 (1) | 11.234(17) | 12.8321(8) | 14.574(3) |
| *c*/Å | 19.195(3) | 19.076(4) | 37.628(3) | 31.52(4) | 22.7982(14) | 18.143(3) |
| *α*/° | 103.00(3) | 102.981(2) | 90 | 90 | 86.824(1) | 68.629(3) |
| *β*/° | 100.75(3) | 100.441(2) | 90 | 94.01(15) | 86.597(1) | 79.220(3) |
| *γ*/° | 97.00(2) | 97.525(1) | 90 | 90 | 79.134(1) | 71.517(3) |
| *U*/Å$^{-3}$ | 2728.9(14) | 2720.5(8) | 14624(2) | 6703(15) | 2838.9(3) | 3177.5(9) |
| *Z* | 2 | 2 | 8 | 4 | 2 | 2 |
| *μ*/mm$^{-1}$ | 0.650 | 0.652 | 0.524 | 0.571 | 0.767 | 0.652 |
| Reflections collected | 23701 | 28916 | 89374 | 35220 | 24825 | 27758 |
| Independent reflections ($R_{int}$) | 9579 (0.0225) | 12399 (0.0381) | 31246 (0.1414) | 11793 (0.6332) | 9978 (0.0563) | 11185 (0.1009) |
| Final *R* indices [$I>2\sigma(I)$]: $R_1$, $wR_2$ | 0.0486, 0.1230 | 0.0496, 0.1210 | 0.0707, 0.1182 | 0.1160, 0.1801 | 0.0571, 0.1368 | 0.0820, 0.1866 |

volume reduced *in vacuo* to *ca.* 15 $cm^3$. After adding toluene (30 $cm^3$) the volume of the solution was reduced *in vacuo* to induce precipitation of a green solid which was thoroughly washed with *n*-hexane (3 × 10 $cm^3$), yield 122 mg (44%).

The complexes *cis*-**19**$^+$[$PF_6$]$^-$, *trans*-**19**$^+$[$PF_6$]$^-$, *cis*-**20**$^+$[$PF_6$]$^-$ and *trans*-**20**$^+$[$PF_6$]$^-$ were prepared similarly.

***trans*-[(dppm)(CO)$_2${(PhO)$_3$P}Mn(μ-NC)Mn(PPh$_3$)(NO)(η$^5$-C$_5$H$_4$Me)][PF$_6$]$_2$ *trans*-1$^{2+}$2[PF$_6$]$^-$.** To a stirred solution of *trans*-[(dppm)(CO)$_2${(PhO)$_3$P}Mn(μ-NC)Mn(PPh$_3$)(NO)(η$^5$-$C_5H_4Me$)][$PF_6$] *trans*-**1**$^+$[$PF_6$]$^-$ (150 mg, 0.133 mmol) in $CH_2Cl_2$ (20 $cm^3$) was added [NO][$PF_6$] (26 mg, 0.146 mmol). After 50 min the resulting purple solution was filtered through Celite, *n*-Hexane (20 $cm^3$) was added and the volume of the solution was reduced *in vacuo* to induce precipitation of a purple solid which was washed with *n*-hexane–$Et_2O$ (1 : 1) (20 $cm^3$) and dried *in vacuo*, yield 93 mg (55%).

The complexes *trans*-**2**$^{2+}$2[$PF_6$]$^-$–**10**$^{2+}$2[$PF_6$]$^-$ were prepared similarly as purple solids.

### Crystal structure determinations of *cis*-2$^+$[PF$_6$]$^-$, *trans*-7$^+$[PF$_6$]$^-$·Me$_2$CO, *cis*-8$^+$[PF$_6$]$^-$·1.5CH$_2$Cl$_2$, *cis*-9$^+$[PF$_6$]$^-$·CH$_2$Cl$_2$, *cis*-12$^+$[PF$_6$]$^-$ and *trans*-17$^+$[PF$_6$]$^-$·Me$_2$CO

Crystals suitable for X-ray diffraction study were grown as follows: orange-red crystals of *cis*-**2**$^+$[$PF_6$]$^-$, *cis*-**8**$^+$[$PF_6$]$^-$·1.5$CH_2Cl_2$, *cis*-**9**$^+$[$PF_6$]$^-$·$CH_2Cl_2$ and *cis*-**12**$^+$[$PF_6$]$^-$, slow diffusion of *n*-hexane into a concentrated $CH_2Cl_2$ solution of the complex at −20 °C; orange-red crystals of *trans*-**7**$^+$[$PF_6$]$^-$·$Me_2CO$ and dark green crystals of *trans*-**17**$^+$[$PF_6$]$^-$·$Me_2CO$, slow diffusion of diethyl ether into an acetone solution of the salt at −20 °C.

Crystals of *trans*-**7**$^+$[$PF_6$]$^-$ and *trans*-**17**$^+$[$PF_6$]$^-$ both contain one molecule of acetone per asymmetric unit, whilst that of *cis*-**8**$^+$[$PF_6$]$^-$ contains 1.5 equivalents of $CH_2Cl_2$ per asymmetric unit and that of *cis*-**9**$^+$[$PF_6$]$^-$ contains one molecule of $CH_2Cl_2$ per asymmetric unit. The Bu$^t$ group of *trans*-**7**$^+$ is rotationally disordered over two positions in an approximately 3 : 1 ratio, and two of the ethyl groups of the P(OEt)$_3$ ligand of *cis*-**8**$^+$ are each disordered over two positions in a 1 : 1 ratio. The structure of *cis*-**9**$^+$ contains two disordered phenyl rings belonging to the dppm ligand, and two disordered OPh groups on the P(OPh)$_3$ ligand. The orientation of the cyanide bridges in all structures was assigned on the basis of the best agreement for the thermal parameters and occupancy factors for the C and N atoms after refinement in two alternative models in which the C and N atoms were exchanged.

For *cis*-**12**$^+$, the crystal also contained disordered solvent molecules which could not be resolved. This was modelled using the programme SQUEEZE,[23] which found the unit cell to contain four voids of 243 Å$^3$, each containing 52 electrons, and four voids of 263 Å$^3$ each containing 48 electrons. This is believed to be due to the presence of highly disordered $CH_2Cl_2$ molecules located within these voids.

Many of the details of the structure analyses are listed in Table 9. CCDC reference numbers 166635, 166636, 644601–644604.

For crystallographic data in CIF or other electronic format see DOI: 10.1039/b705975b

## Acknowledgements

We thank the University of Bristol for Postgraduate Scholarships (K.M.A., E.L.-R.), the Leverhulme Foundation for a Postdoctoral Fellowship (R.L.P.) and Professor M.D. Ward for providing facilities for the spectroelectrochemical studies.

## References

1 G. A. Carriedo, N. G. Connelly, M. C. Crespo, I. C. Quarmby, V. Riera and G. H. Worth, *J. Chem. Soc., Dalton Trans.*, 1991, 315.
2 G. A. Carriedo, N. G. Connelly, S. Alvarez, E. Perez-Carreno and S. Garcia-Granda, *Inorg. Chem.*, 1993, **32**, 272.
3 C. J. Adams, K. M. Anderson, M. Bardaji, N. G. Connelly, N. J. Goodwin, E. Llamas-Rey, A. G. Orpen and P. H. Rieger, *Dalton Trans.*, 2004, 683.
4 K. M. Anderson, N. G. Connelly, E. Llamas-Rey, A. G. Orpen and R. L. Paul, *Chem. Commun.*, 2001, 1734.
5 N. G. Connelly, K. A. Hassard, B. J. Dunne, A. G. Orpen, S. J. Raven, G. A. Carriedo and V. Riera, *J. Chem. Soc., Dalton Trans.*, 1988, 1623; C. F. Hogan, A. M Bond, A. K. Neufeld, N. G. Connelly and E. Llamas-Rey, *J. Phys. Chem. A*, 2003, **107**, 1274.
6 D. A. Dows, A. Haim and W. K. Walmarth, *J. Inorg. Nucl. Chem.*, 1961, **21**, 33.
7 S. F. A. Kettle, E. Diana, E. Boccaleri and P. L. Stanghellini, *Inorg. Chem.*, 2007, **46**, 2409.
8 A. J. Deeming, G. P. Proud, H. M. Dawes and M. B. Hursthouse, *Polyhedron*, 1988, **7**, 651.
9 D. J. Darensbourg, J. C. Yoder, M. W. Holtcamp, K. K. Klausmeyer and J. H. Reibenspies, *Inorg. Chem.*, 1996, **35**, 4764.
10 F. R. Fronczek and W. P. Schaefer, *Inorg. Chem.*, 1974, **13**, 727.
11 N. Zhu and H. Vahrenkamp, *Angew. Chem., Int. Ed. Engl.*, 1994, **33**, 2090.
12 Cambridge Structural Database, version 5.21, CCDC, April 2002.
13 C. J. Adams, N. G. Connelly, N. J. Goodwin, O. D. Hayward, A. G. Orpen and A. J. Wood, *Dalton Trans.*, 2006, 3584.
14 A. Geiss, M. J. Kolm, C. Janiak and H. Vahrenkamp, *Inorg. Chem.*, 2000, **39**, 4037.
15 N. S. Hush, *Prog. Inorg. Chem.*, 1967, **8**, 391; N. S. Hush, *Coord. Chem. Rev.*, 1985, **64**, 135.
16 N. G. Connelly, O. M. Hicks, G. R. Lewis, A. G. Orpen and A. J. Wood, *Chem. Commun.*, 1998, 517.
17 G. A. Carriedo, M. C. Crespo, V. Riera, M. G. Sanchez, M. L. Valin, D. Moreiras and X. Solans, *J. Organomet. Chem.*, 1986, **302**, 47.
18 F. Bombin, G. A. Carriedo, J. A. Miguel and V. Riera, *J. Chem. Soc., Dalton Trans.*, 1981, 2049.
19 T. A. James and J. A. McCleverty, *J. Chem. Soc. A*, 1970, 850.
20 D. Bellamy, N. G. Connelly, O. M. Hicks and A. G. Orpen, *J. Chem. Soc., Dalton Trans.*, 1999, 3190.
21 D. L. Reger, D. J. Fauth and M. D. Dukes, *J. Organomet. Chem.*, 1979, **170**, 217.
22 N. G. Connelly and W. E. Geiger, *Chem. Rev.*, 1996, **96**, 877.
23 A. L. Spek, *SQUEEZE, incorporated into PLATON: A Multipurpose Crystallographic Tool*, Utrecht University, Utrecht, The Netherlands, 2005.

 